Research Square

Preprints are preliminary reports that have not undergone peer review.
They should not be considered conclusive, used to inform clinical practice,
or referenced by the media as validated information.

Tetramethylpyrazine ameliorates ulcerative colitis via B. pseudolongum-driven taurine metabolism and M2 macrophage polarization

Zhijiang Huang
2nd Abdominal Surgery Department, Jiangxi Cancer Hospital, The Second Affiliated Hospital of Nanchang Medical College

Xiaojian Zhu
2nd Abdominal Surgery Department, Jiangxi Cancer Hospital, The Second Affiliated Hospital of Nanchang Medical College

Yanglin Chen
2nd Abdominal Surgery Department, Jiangxi Cancer Hospital, The Second Affiliated Hospital of Nanchang Medical College

Hongtao Wan
2nd Abdominal Surgery Department, Jiangxi Cancer Hospital, The Second Affiliated Hospital of Nanchang Medical College

Dengke Yao
2nd Abdominal Surgery Department, Jiangxi Cancer Hospital, The Second Affiliated Hospital of Nanchang Medical College

Min Peng
2nd Abdominal Surgery Department, Jiangxi Cancer Hospital, The Second Affiliated Hospital of Nanchang Medical College

Xujie Deng
2nd Abdominal Surgery Department, Jiangxi Cancer Hospital, The Second Affiliated Hospital of Nanchang Medical College

Jiangfeng Yin
2nd Abdominal Surgery Department, Jiangxi Cancer Hospital, The Second Affiliated Hospital of Nanchang Medical College

Xianwu Zhang
2nd Abdominal Surgery Department, Jiangxi Cancer Hospital, The Second Affiliated Hospital of Nanchang Medical College

Yu He
2nd Abdominal Surgery Department, Jiangxi Cancer Hospital, The Second Affiliated Hospital of Nanchang Medical College

Jianyong Xiong

2nd Abdominal Surgery Department, Jiangxi Cancer Hospital, The Second Affiliated Hospital of Nanchang Medical College

Faming Zhang

Department of Microbiota Medicine & Medical Center for Digestive Diseases The Second Affiliated Hospital of Nanjing Medical University Nanjing China

Dan Liu

Jiangxi Province Key Laboratory of Drug Target Discovery and Validation, School of Pharmacy, Jiangxi Medical College

Bo Yi

yibo@ncmc.edu.cn

2nd Abdominal Surgery Department, Jiangxi Cancer Hospital, The Second Affiliated Hospital of Nanchang Medical College

---

Research Article

Keywords: Ulcerative colitis, Tetramethylpyrazine, Bifidobacterium pseudolongum, Taurine metabolism, Macrophage polarization, Foxo1 signaling

Posted Date: July 30th, 2026

DOI: https://doi.org/10.21203/rs.3.rs-10454410/v1

License: This work is licensed under a Creative Commons Attribution 4.0 International License. Read Full License

Additional Declarations: No competing interests reported.

Tetramethylpyrazine ameliorates ulcerative colitis via *B. pseudolongum*-driven taurine metabolism and M2 macrophage polarization

Zhijiang Huang[#,1,2,3], Xiaojian Zhu[#,1], Yanglin Chen[#,1], Hongtao Wan[#,1], Dengke Yao[1,2,3], Min Peng[1,2,3], Xujie Deng[1,2,3], Jiangfeng Yin[1,2,3], Xianwu Zhang[1,2,3], Yu He[1,2,3], Jianyong Xiong[1], Faming Zhang[4], Dan Liu[5,6*], Bo Yi[1,7*]

[1]2nd Abdominal Surgery Department, Jiangxi Cancer Hospital, The Second Affiliated Hospital of Nanchang Medical College, Nanchang, Jiangxi, 330029, P.R. China.

[2]Jiangxi Medical College, Nanchang University, Nanchang, Jiangxi, 330006, P.R. China.

[3]Jiangxi Key Laboratory of Oncology, Jiangxi Cancer Hospital, Nanchang 330006, P.R. China.

[4]Department of Microbiota Medicine & Medical Center for Digestive Diseases The Second Affiliated Hospital of Nanjing Medical University Nanjing China.

[5]Jiangxi Province Key Laboratory of Drug Target Discovery and Validation, School of Pharmacy, Jiangxi Medical College, Nanchang University, Nanchang, China.

[6]The MOE Basic Research and Innovation Center for the Targeted Therapeutics of Solid Tumors, School of Pharmacy, Jiangxi Medical College, Nanchang University, Nanchang, China.

[7]Jiangxi Provincial Key Clinical Specialty Construction Project-Colorectal Cancer Center, Jiangxi Cancer Hospital, The Second Affiliated Hospital of Nanchang Medical College, Nanchang, Jiangxi, 330029, P.R. China.

[#]These authors contributed equally to this work.

[*]Correspondence: Professor Dan Liu and Bo Yi.

Bo Yi acted as a lead contact.

Email: Dan Liu, liudan1201jx@ncu.edu.cn; Bo Yi, yibo@ncmc.edu.cn.

Abstract:

Ulcerative colitis (UC), a chronic and relapsing inflammatory disorder of the colon, stems from dysregulated interactions between host immunity and the gut microbiota. However, precise pharmacomicrobiomics targets that modulate this interaction remain poorly characterized. Here, we identify Tetramethylpyrazine (TMP) as a potent suppressor of intestinal inflammation in murine colitis models, a protective effect contingent upon the induction of anti-inflammatory macrophage M2 polarization. Integrated 16S rRNA sequencing reveals that TMP reconfigures the gut microbial architecture, augmenting both α- and β-diversity while selectively enriching *Bifidobacterium pseudolongum*. Crucially, *B. pseudolongum* abundance inversely correlates with disease severity. Using gnotobiotic mouse models and fecal microbiota transplantation (FMT), we causally demonstrate that the anti-inflammatory efficacy of TMP is strictly microbiota-dependent and can be recapitulated by *B. pseudolongum* alone. Untargeted metabolomics further uncovers that *B. pseudolongum* remodels the host metabolic landscape, specifically promoting the accumulation of taurine and N-stearoyl taurine. Mechanistically, we delineate how *B. pseudolongum* reprograms host taurine metabolism to activate the Foxo1-mediated oxidative stress response, culminating in the upregulation of Sesn3, Sod2, and Cat antioxidant defenses that orchestrate macrophage M2 polarization. This immunomodulatory cascade proves indispensable for TMP-mediated protection against colitis. Collectively, our findings unveil a previously unrecognized gut microbiota-host metabolic circuit wherein TMP ameliorates UC through *B. pseudolongum*-driven taurine metabolism and subsequent macrophage M2 polarization, highlighting novel therapeutic avenues for targeting microbial-metabolic-immune networks in inflammatory diseases.

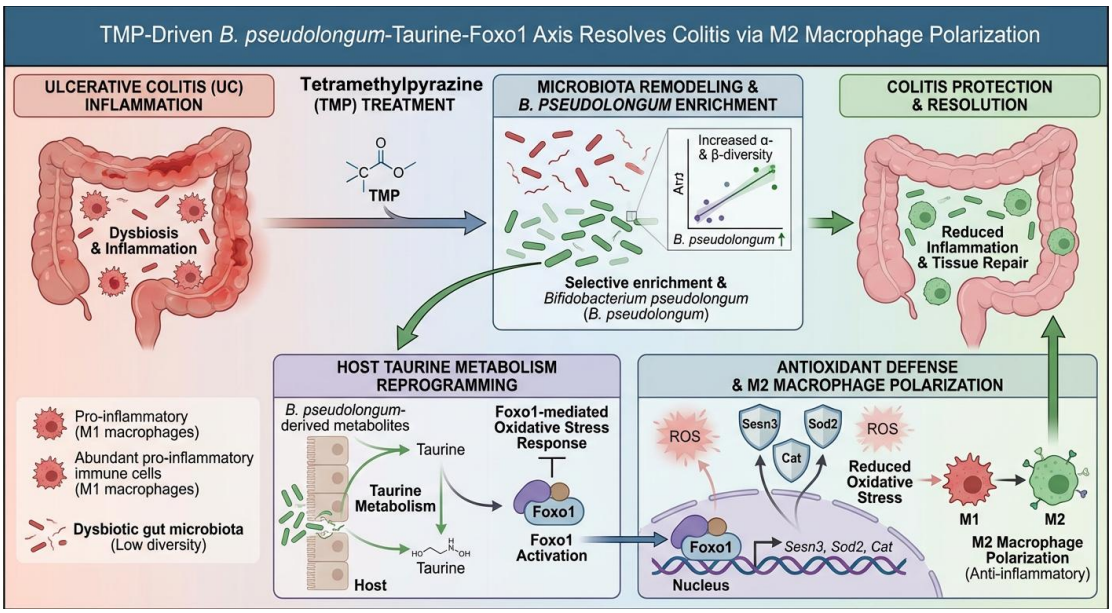
Key words:

Ulcerative colitis; Tetramethylpyrazine; *Bifidobacterium pseudolongum*; Taurine metabolism; Macrophage polarization; Foxo1 signaling

Highlights:

- TMP resolves colitis by acting as a microbial ecosystem engineer to selectively enrich *B. pseudolongum*.
- Gnotobiotic and FMT assays confirm a causal *B. pseudolongum*-taurine axis that reprograms the host metabolic landscape.
- Mechanistically, bacterial-derived taurine activates Foxo1-mediated antioxidant defenses (Sesn3/Sod2/Cat) to license restorative M2 macrophage polarization.

Graphical Abstract



Introduction

Ulcerative colitis (UC) marks a catastrophic failure of the homeostatic dialogue between the host immune system and the commensal microbiota. While biologic therapies targeting cytokine and integrin signaling have transformed patient care, primary non-response rates approaching 40% underscore the inherent limitations of treating the host in isolation [1, 2]. The pathogenesis of UC is inextricably linked to the collapse of the “meta-organism”, wherein the depletion of specific microbial metabolites starves the mucosal immune system of essential regulatory signals [3–5]. In this context, Tetramethylpyrazine (TMP), a bioactive pyrazine alkaloid, has demonstrated potent anti-inflammatory efficacy [6–8]. However, a critical mechanistic gap persists in the field of pharmacomicrobiomics: does TMP exert its effects solely through intrinsic pharmacology, or does it act as a "microbial ecosystem engineer," resolving inflammation by reconstituting the disrupted metabolic dialogue between commensals and host immunity?

Central to mucosal repair is the metabolic repolarization of macrophages [9–11]. These sentinel cells must transition from a glycolytic, pro-inflammatory M1 state to an oxidative phosphorylation-dependent, tissue-restorative M2 phenotype [12, 13]. This phenotypic switch is strictly gated by cellular redox status; excessive reactive oxygen species (ROS) disrupt the mitochondrial integrity required for M2 polarization, perpetuating a vicious cycle of chronic inflammation [14–16]. Consequently, the transcriptional machinery coupling antioxidant defense with metabolic reprogramming represents a critical checkpoint in disease resolution. While microbial metabolites such as short-chain fatty acids are known to modulate T cell differentiation, the specific microbial cues-particularly amino acid derivatives-that license this antioxidant-driven macrophage plasticity remain elusive [17–19].

Here, we demonstrate that TMP resolves colitis not by directly engaging host receptors, but by selectively enriching the commensal *Bifidobacterium pseudolongum*. Using gnotobiotic models and fecal microbiota transplantation (FMT), we establish that *B.*

pseudolongum is both necessary and sufficient to recapitulate the protective phenotype. Mechanistically, we reveal that *B. pseudolongum* rewires the gut metabolic landscape to elevate taurine availability. This metabolic input potentiates the host Foxo1 signaling axis, triggering a transcriptional antioxidant program—upregulating *Sesn3*, *Sod2*, and *Cat*—that functions as a metabolic rheostat. This suppression of oxidative stress subsequently licenses restorative M2 macrophage polarization. Collectively, our findings identify a cross-kingdom mechanism by which a pharmacological agent leverages microbial metabolism to orchestrate immune resolution. These data suggest that the host has evolutionarily "outsourced" critical aspects of tissue repair to the microbiota, offering a paradigm for treating refractory inflammatory bowel disease (IBD) by targeting the holobiont network rather than the host or microbe in isolation.

Results

TMP confers protection against DSS-induced colitis by preserving intestinal barrier architecture and mucosal homeostasis

To rigorously evaluate the therapeutic efficacy of TMP in the context of ulcerative colitis, we utilized a DSS-induced murine model of acute epithelial injury [20, 21]. Mice were randomized into vehicle, DSS-only, Sulfasalazine (SASP, positive control), low-dose TMP (L-TMP, 20 mg/kg), and high-dose TMP (H-TMP, 40 mg/kg) cohorts (**Figure 1a**). While DSS challenge precipitated a precipitous decline in body weight starting on day 8, intervention with TMP significantly attenuated this cachectic response in a dose-dependent manner. Notably, the efficacy of H-TMP was comparable to that of the clinical standard SASP (**Figure 1b**). Consistent with these macroscopic observations, the disease activity index (DAI)-a composite metric integrating weight loss, stool consistency, and rectal bleeding-was robustly suppressed by TMP treatment (**Figure 1c**). Furthermore, colonic shortening was normalized to near-baseline levels, while splenomegaly—a hallmark of systemic immune activation—was significantly ameliorated in the H-TMP cohort (**Figure 1d-g**).

Histopathological assessment confirmed that TMP conferred profound cytoprotection. H&E staining revealed that while DSS exposure caused extensive epithelial erosion, crypt distortion, and neutrophilic infiltration, TMP treatment preserved the crypt-villus architecture and significantly reduced inflammatory scores (**Figure 1h; Figure S1a**). To dissect the impact on barrier integrity, we examined the mucus layer and apical junctional complex. AB-PAS staining and MUC-2 immunohistochemistry demonstrated that TMP rescued the DSS-induced depletion of goblet cells and mucin production (**Figure 1i, j; Figure S1b, c**). At the molecular level, Western blot analysis confirmed that the expression of critical tight junction proteins-ZO-1, Occludin, and Claudin-5-was severely compromised by DSS but dose-dependently restored by TMP (**Figure 1k; Figure S1d-f**).

Collectively, these data establish that TMP confers robust protection against DSS-induced colitis, effectively normalizing clinical and histological indices of disease severity. By restoring the structural integrity of the apical junctional complex and reinstating mucin production, TMP reinforces the intestinal barrier, thereby positioning it as a potent therapeutic agent for resolving mucosal inflammation.

TMP orchestrates anti-inflammatory and immunomodulatory programs in DSS-induced colitis

To elucidate the molecular circuitry underpinning TMP-mediated protection, we profiled the colonic transcriptome via RNA sequencing. Pathway enrichment analysis unveiled a distinct dual mechanism: TMP treatment concurrently attenuated inflammatory signaling (e.g., IL-17, Th1/Th2 differentiation) while restoring metabolic homeostasis (e.g., oxidative phosphorylation, TCA cycle) (**Figure 2a**). Substantiating this regulatory shift, Gene Set Enrichment Analysis (GSEA) revealed a robust negative enrichment of signatures defining "Inflammatory Bowel Disease" (NES = –1.56, P = 0.02) and type 1 immunity (NES = –1.41, P = 0.03) in TMP-treated mice (**Figure 2b, d, e**). This transcriptional repression selectively targeted key effectors of the Th17 axis—including *Il17a*, *Il17f*, and *Il6*—thereby dismantling the pro-inflammatory cascade (**Figure 2f, g**). Conversely, gene sets governing "Gastrointestinal Epithelial Maintenance" and "Oxidative Phosphorylation" were significantly enriched (NES = 1.58, P = 0.02), aligning with our histological evidence of accelerated mucosal repair and bioenergetic recovery (**Figure 2c, h**).

Validating these transcriptomic signatures at the cellular level, immunofluorescence analysis demonstrated that TMP treatment reversed the DSS-induced skewing of macrophages toward a pro-inflammatory M1 state (**F4/80$^+$CD86$^+$**). Strikingly, TMP not only suppressed M1 markers but actively promoted a shift toward the restorative M2 phenotype (**F4/80$^+$CD163$^+$**) (**Figure 2i–l**). This immunomodulatory reprogramming was corroborated by cytokine profiling, which showed a pronounced attenuation of TNF-α, IL-1β, and IL-6, alongside an upregulation of the anti-inflammatory cytokine

IL-10 (**Figure 2m, n; Figure S2a, b**). Collectively, these multi-omics data establish TMP as a pivotal regulator that resolves colitis by extinguishing Th1/Th17-driven inflammation while recalibrating macrophage polarization to favor a pro-resolution microenvironment.

TMP drives a global reconstruction of the gut microbiome and specifically enriches *B. pseudolongum*

To determine whether gut ecosystem reconfiguration underpins the therapeutic efficacy of TMP, we performed 16S rRNA gene sequencing on fecal samples from Control, DSS-challenged, and TMP-treated cohorts. Evaluation of α-diversity metrics demonstrated that DSS challenge precipitated a severe collapse in microbial richness and evenness, evidenced by significantly diminished Shannon and Simpson indices (**Figure 3a, b**). Strikingly, TMP intervention abrogated this dysbiosis, restoring community diversity to levels indistinguishable from the homeostatic state. This recovery of microbial architecture was corroborated by Principal Coordinate Analysis (PCoA), which revealed distinct stratification among groups (**Figure 3c**). Multivariate permutation analysis confirmed that TMP treatment drives a potent reshaping of the global microbiome landscape, segregating the TMP cohort clearly from DSS-associated dysbiosis (Adonis $R^2 = 0.446$, $P = 0.001$).

Taxonomic profiling delineated the specific compositional shifts governing these community dynamics. The DSS-induced state was characterized by a classic inflammatory signature, comprising a contraction of beneficial Firmicutes concomitant with an expansion of *Proteobacteria, Bacteroidota*, and *Verrucomicrobiota* (**Figure 3d, f**). TMP administration successfully reversed this imbalance, recapitulating a phylum-level profile that mirrors the healthy control phenotype. At finer taxonomic resolutions, heatmaps and stacked bar plots highlighted a profound restructuring of the microbial community (**Figure 3e, g; Figure S3a, b**). Specifically, TMP treatment not only curtailed the bloom of opportunistic pathobionts associated with colitis but also substantially replenished key commensal genera depleted by DSS challenge.

To identify specific microbial drivers of this community differentiation, we employed Linear Discriminant Analysis Effect Size (LEfSe) (**Figure 3h**). This analysis pinpointed distinct taxonomic signatures for each group: while the DSS phenotype was defined by an enrichment of opportunistic taxa (e.g., *Clostridiales bacterium*), the TMP-treated group was notably enriched with beneficial commensals, including *Akkermansia muciniphila* and *B. pseudolongum*. Quantitative validation confirmed that the relative abundances of *B. pseudolongum* (**Figure 3i**) and *A. muciniphil*a (**Figure 3j**), which were significantly suppressed under DSS conditions, were robustly rescued following TMP treatment ($P < 0.01$ and $P < 0.05$, respectively). Consistently, TMP significantly restored the abundance of taxa such as *Clostridiales bacterium* and *gut metagenome* (**Figure 3k, l**), reinforcing the conclusion that TMP promotes the recovery of beneficial commensals.

To interrogate the functional relevance of these specific microbial shifts, we analyzed the microbiome-phenotype axis via correlation analysis. Notably, among the identified key taxa, *B. pseudolongum* emerged as a pivotal correlate of host health. Its abundance exhibited a strong positive correlation with body weight ($R = 0.9484$, $P = 0.0003$; **Figure 3m**) and colon length ($R = 0.9715$, $P < 0.0001$; **Figure 3o**), while showing a potent negative correlation with the DAI ($R = -0.9073$, $P = 0.0019$; **Figure 3n**) and spleen coefficient ($R = -0.9662$, $P < 0.0001$; **Figure 3p**). In contrast, other modulated taxa, including *A. muciniphila*, failed to show significant linear associations with these clinical parameters (**Figure S3c–e**).

Corroborating the translational significance of these murine findings, we analyzed a clinical cohort from The Second Affiliated Hospital of Nanjing Medical University. Consistent with our murine data, *B. pseudolongum* abundance was significantly depleted in patients with ulcerative colitis compared to healthy controls ($P = 0.004$; **Figure S3f**). Moreover, in human subjects, the abundance of this bacterium displayed significant negative correlations with key clinical indices of disease severity and inflammation, including the Mayo score ($R = -0.454$, $P = 0.017$), C-reactive protein

(CRP; R = -0.398, P = 0.040), white blood cell count (WBC; R = -0.404, P = 0.037), and erythrocyte sedimentation rate (ESR; R = -0.387, P = 0.046; **Figure S3f**). Collectively, these data identify *B. pseudolongum* as a key responder to TMP treatment that is intimately linked to the amelioration of colitis, demonstrating a conserved microbe-host interaction mechanism across species.

The therapeutic effect of TMP on DSS-induced colitis is microbiota-dependent

Given that TMP robustly ameliorates colitis while simultaneously reshaping the gut ecosystem, a critical mechanistic question remains: is this microbial reconstruction causal or merely correlative? To determine whether the gut microbiota is indispensable for TMP-mediated protection, we depleted the commensal community using a broad-spectrum antibiotic cocktail (ABX) prior to and during DSS challenge (**Figure 4a**) [22, 23]. This approach allowed us to rigorously dissect the dependency of TMP efficacy on microbial presence.

Comprehensive 16S rRNA gene sequencing confirmed that ABX treatment precipitated a profound collapse of the microbial community, evidenced by distinct segregation in Principal Coordinate Analysis (PCoA) (Adonis R^2 = 0.566, P = 0.003; **Figure 4b**). Crucially, this depletion effectively nullified the compositional shifts typically induced by TMP. In the ABX-treated cohort, TMP failed to elicit discernible changes in alpha diversity (Shannon and Simpson indices) and remained significantly lower than the non-antibiotic DSS+TMP cohort (**Figure 4c, d**), demonstrating that TMP's ecological impact is strictly dependent on a baseline microbial community. At finer taxonomic resolutions, the distinct microbial signatures previously associated with TMP treatment—including *Clostridium sp*, *Clostridium leptum*, and *Lactobacillus reuteri*—were abolished in the antibiotic background (**Figure 4e; Figure S4a, b**), confirming the absence of substrate for TMP-driven modulation.

We next assessed whether this loss of microbial responsiveness translated to a loss of therapeutic efficacy. Strikingly, microbiota depletion completely abrogated the

protective effects of TMP against DSS-induced colitis. ABX-treated mice receiving TMP exhibited exacerbated disease pathology comparable to untreated controls, characterized by accelerated body weight loss (**Figure 4f**), elevated DAI scores (**Figure 4g**), pronounced colon shortening (**Figure 4h**), and increased splenomegaly (**Figure 4i**).

To elucidate the downstream consequences of this microbial dependence, we interrogated the intestinal barrier and immune landscape. Molecular analysis revealed that the TMP-induced restoration of tight junction proteins (ZO-1, Occludin, and Claudin-5) was compromised in the absence of a functional microbiota (**Figure 4j; Figure S4c-e**). Furthermore, the immunomodulatory capacity of TMP was severely impaired; ABX treatment prevented the TMP-driven shift toward a restorative M2 macrophage phenotype ($CD163^+$), instead maintaining a pro-inflammatory M1 profile ($CD86^+$) within the colonic mucosa (**Figure 4k, m; Figure S4f-j, n, o**). Consistently, histopathological assessment demonstrated that without an intact microbiota, TMP failed to rescue epithelial architecture or mucin production (MUC-2, AB-PAS) (**Figure 4l; Figure S4k-m**). Collectively, these data establish that the gut microbiota is not merely a passenger but an essential mediator of TMP's therapeutic effects on barrier integrity and immune homeostasis.

TMP coordinates a *B. pseudolongum*-dependent metabolic axis via N-stearoyl Taurine and host TauT activation

Having established the structural restoration of the gut microbiota by TMP, we sought to elucidate the functional consequences of this microbial reconfiguration and its mechanistic interplay with host metabolism. To map the phylogenetic origins of metabolic alterations, we constructed a Sankey diagram tracing the taxonomic lineage of key responders. This analysis highlighted a robust enrichment of the *Bifidobacteriaceae* family, specifically the species ***Bifidobacterium pseudolongum*** (***B. pseudolongum***), in the TMP-treated group, linking this taxon to potential taurine-associated metabolic outputs (**Figure S5a**). Concomitantly, GSEA of the transcriptomic

profile revealed a significant upregulation of the "Amino Acid Biosynthetic Process" (NES = 1.34, $P = 0.02$) in TMP-treated mice, driven by core metabolic genes such as Aldh1a1 and Gad2 (**Figure S5b**).

To identify the specific metabolic effectors mediating the protective effects of TMP, we performed untargeted metabolomics profiling. The analysis unveiled a profound metabolic shift, with N-Stearoyl Taurine emerging as a top-ranking differential metabolite significantly upregulated by TMP intervention compared to the DSS-challenged group (**Figure 5a**). To interrogate the crosstalk between the rescued microbiome and this metabolic reprogramming, we generated a multi-omics correlation heatmap. Strikingly, *B. pseudolongum* exhibited a highly specific and positive correlation with N-Stearoyl Taurine levels ($P < 0.001$), suggesting that this commensal may drive the biosynthesis or accumulation of this specific taurine conjugate (**Figure 5b**).

Given the prominence of taurine-conjugated lipids, we hypothesized that TMP might modulate host taurine homeostasis mechanisms. Indeed, GSEA identified a significant enrichment of the "Taurine Transport" pathway (NES = 1.69, $P < 0.001$) in the colonic tissue of TMP-treated mice (**Figure 5c**). We next validated the expression of specific taurine transporters. RNA-seq analysis demonstrated that TMP selectively restored the mRNA expression of *Slc6a6* (encoding the Taurine Transporter, TauT), which was significantly suppressed by DSS ($P < 0.01$), whereas the expression of alternative transporters *Slc6a12* and *Slc6a13* remained unaltered (**Figure S5c**).

At the translational level, immunoblotting confirmed that TMP treatment effectively reversed the DSS-induced depletion of TauT protein, restoring expression to levels comparable to the SASP positive control (**Figure 5d**). Furthermore, immunofluorescence staining of colonic sections corroborated these findings, revealing that TMP preserved the apical membrane localization and abundance of TauT in colonic epithelial cells, contrasting sharply with the diminished signal observed in the DSS group (**Figure 5e**).

Collectively, these multi-omics data define a novel therapeutic axis wherein TMP promotes the expansion of *B. pseudolongum* and the accumulation of N-Stearoyl Taurine, which acts in concert with restored host TauT expression to reinforce intestinal homeostasis.

The therapeutic efficacy of TMP is contingent upon a *B. pseudolongum*-driven taurine metabolic axis

To definitively establish the causal contribution of the gut microbiota—specifically Bifidobacterium—to the therapeutic efficacy of TMP, we utilized a pseudo-germ-free (PGF) murine model established via broad-spectrum antibiotic (ABX) depletion prior to DSS challenge (**Figure 6a**). In this microbiota-deficient landscape, we assessed whether recolonization with ***B. pseudolongum* (*Bifi.*)** or supplementation with its downstream metabolite, taurine (Tau.), could rescue or potentiate the protective effects of TMP. 16S rRNA sequencing confirmed the successful colonization and specific enrichment of Bifidobacterium pseudolongum in the reconstituted groups (**Figure S6a, b**) [24, 25].

Clinical monitoring revealed that while ABX-treated DSS mice exhibited severe wasting disease, TMP administration alone in this microbiota-depleted setting conferred only partial protection. Strikingly, the co-administration of *B. pseudolongum* and TMP (ABX+DSS+*Bifi.*+TMP) significantly potentiated therapeutic efficacy, arresting body weight loss and suppressing the DAI more robustly than either monotherapy (**Figure 6b, c**). Crucially, exogenous supplementation with taurine in TMP-treated mice (ABX+DSS+TMP+Taurine) was sufficient to recapitulate the maximal protective phenotype observed in the *B. pseudolongum*-reconstituted group, effectively bypassing the requirement for bacterial colonization. This functional redundancy strongly implies that taurine is the critical metabolic effector of the TMP-*B. pseudolongum* axis.

Macroscopic and systemic assessments further corroborated this mechanistic link. The

colonic shortening and splenomegaly induced by DSS were significantly ameliorated in the *Bifi.*+TMP and TMP+Taurine cohorts, with efficacy superior to that of the TMP-only group in the ABX background (**Figure 6d-g**). Histological analysis (H&E) confirmed that while DSS provoked extensive epithelial erosion and inflammatory infiltration, the synergistic application of TMP with either *B. pseudolongum* or taurine preserved the crypt-villus architecture (**Figure 6h**). Furthermore, assessment of the chemical barrier via AB-PAS staining and MUC-2 immunohistochemistry demonstrated that these combinatorial interventions robustly restored goblet cell numbers and mucin secretion, reinforcing the mucosal barrier against luminal insults (**Figure 6h**).

To delineate the molecular mechanism underlying this barrier restoration, we examined the expression of tight junction proteins and the taurine transporter (TauT). Western blot analysis revealed that DSS exposure downregulated ZO-1, Occludin, and Claudin-5, a defect that was reversed by *B. pseudolongum* or taurine supplementation. Notably, the expression of TauT was markedly upregulated in the treatment groups, suggesting enhanced host uptake of microbial-derived taurine (**Figure S6e, g**).

Finally, to determine whether this microbe-metabolite axis reprograms the immune microenvironment, we examined macrophage polarization. In the ABX+DSS colon, we observed a profound infiltration of $CD86^+$ pro-inflammatory macrophages (M1-like) and a scarcity of $CD163^+$ anti-inflammatory macrophages (M2-like). Notably, treatment with TMP alongside *B. pseudolongum* or taurine significantly abrogated the M1 inflammatory influx (**Figure 6i**) and reciprocally promoted M2 polarization (**Figure S6c, d**). This immunomodulatory shift was substantiated by protein-level analysis, which showed a suppression of pro-inflammatory cytokines (TNF-α) and an elevation of regulatory cytokines (IL-10, TGF-β) (**Figure S6f**).

Collectively, these data provide definitive causal evidence that the anti-colitic efficacy of TMP is not autonomous but relies on a tripartite "TMP–*B. pseudolongum*–Taurine" axis. Specifically, TMP promotes the expansion of *B. pseudolongum*, which in turn

supplies taurine to upregulate TauT, resolve mucosal inflammation via M2 macrophage polarization, and reinforce the epithelial barrier.

Taurine modulates macrophage polarization and inflammatory response via Foxo1 signaling pathway

To delineate the molecular mechanisms by which taurine regulates macrophage plasticity, we integrated transcriptomic profiling with functional validation. RNA sequencing of colonic tissues revealed that TMP treatment significantly reversed DSS-induced gene expression signatures (**Figure 7a, b**). Pathway enrichment analysis identified the FoxO signaling pathway as a top candidate mediating these effects (**Figure 7c, d**). Furthermore, correlation analysis (Mantel-test) demonstrated significant linkages between the FoxO pathway and specific metabolites, including N-Stearoyl Taurine and *Sesn3*, suggesting that taurine-associated metabolites may directly influence macrophage biology through this signaling node (**Figure 7e**).

We validated the relevance of Foxo1 signaling through a series of in vivo experiments. Initial immunoblotting confirmed that TMP treatment suppressed DSS-altered Foxo1 phosphorylation (**Figure 7f**). Subsequent experiments involving antibiotic (ABX) pretreatment and Bifidobacterium recolonization demonstrated that the protective effects of the microbiota were intrinsically associated with reduced p-Foxo1 level (**Figure 7g, h**). Critically, direct supplementation with taurine recapitulated these modulatory effects on Foxo1 signaling, thereby establishing a direct link between the metabolite and the pathway (**Figure 7i, j**).

In vitro studies using RAW264.7 macrophages confirmed that taurine promoted a shift toward an anti-inflammatory M2-like phenotype upon LPS stimulation, evidenced by altered polarization markers and cytokine profiles (**Figure 7k, l**). The pivotal role of Foxo1 was substantiated using the specific inhibitor AS1842856. While the inhibitor alone did not affect cell viability at low concentrations (**Figure 7m, n**), it effectively abrogated taurine-mediated nuclear translocation of Foxo1 (**Figure 7p**) and reversed

the anti-inflammatory polarization profile (**Figure 7q, r**).

Supplementary analyses provided further mechanistic insight into the downstream effectors. Taurine treatment upregulated the expression of key antioxidant enzymes-Sesn3, Cat, and Sod2-and significantly reduced LPS-induced intracellular ROS levels (**Figure 7o; Figure S7c-e**). Importantly, the Foxo1 inhibitor partially reversed these antioxidant effects and ROS scavenging (**Figure S7d, e**). In summary, our multi-faceted data establish that taurine drives anti-inflammatory macrophage polarization primarily through a Foxo1-dependent regulation of the intracellular redox environment.

Taurine supplementation alleviates colitis by reinforcing intestinal barrier integrity and skewing macrophage polarization

To validate the functional relevance of taurine in UC pathogenesis, we administered exogenous taurine to DSS-challenged mice, either alone or in combination with TMP (**Figure 8a**). Taurine supplementation significantly abrogated the severity of colitis, as evidenced by the preservation of body weight and a marked reduction in DAI scores compared to the DSS vehicle group (**Figure 8b, c**). Macroscopic assessment further corroborated these protective effects; taurine treatment effectively prevented colonic shortening and suppressed splenomegaly, indicative of a robust containment of both local tissue injury and systemic inflammation (**Figure 8d-g**).

Mechanistically, we sought to determine whether taurine restores epithelial barrier function. Immunoblotting revealed that while DSS challenge severely compromised the expression of tight junction proteins—ZO-1, Occludin, and Claudin-5—taurine administration rescued these critical barrier components (**Figure 8h**). Beyond the epithelial barrier, we investigated the immunomodulatory potential of taurine, specifically focusing on macrophage plasticity. Strikingly, taurine treatment orchestrated a shift in macrophage polarization towards an anti-inflammatory M2 phenotype, characterized by upregulated CD163 expression and suppressed Foxo1 phosphorylation, alongside downregulated CD86 (M1 marker) [26]. This phenotypic

skewing was accompanied by a rebalancing of the cytokine milieu, favoring anti-inflammatory mediators (TGF-β, IL-10) over pro-inflammatory cytokines (TNF-α) (**Figure 8i**).

Histological analysis confirmed that these molecular changes translated into structural protection, with taurine-treated mice exhibiting preserved mucosal architecture and minimized inflammatory infiltration (**Figure 8j-l**). Collectively, these findings establish that taurine confers protection against colitis through a dual mechanism involving the restoration of epithelial integrity and the promotion of an anti-inflammatory macrophage phenotype.

Discussion

Our study unveils a sophisticated trans-kingdom signaling axis wherein TMP resolves UC not through direct immunosuppression, but by recalibrating the host-microbe metabolic dialogue. We identify *B. pseudolongum* as the pivotal microbial architect that, through taurine metabolic reprogramming, engages a host Foxo1-dependent antioxidant program to enforce an anti-inflammatory M2 macrophage phenotype. This finding represents a conceptual advance in pharmacomicrobiomics, moving beyond the cataloging of dysbiotic signatures to elucidate a causal, mechanistically defined circuit linking specific commensal metabolism to immune cell plasticity.

While generalized restoration of microbial diversity is a hallmark of recovery, our data argue for a deterministic role of *B. pseudolongum*. By transitioning from correlation to causation via germ-free colonization and FMT, we establish that *B. pseudolongum* is sufficient to recapitulate the therapeutic efficacy of TMP. This elevates the bacterium from a passive biomarker to an active therapeutic agent. Unlike *A. muciniphila*, which primarily reinforces physical barriers, *B. pseudolongum* appears to function as a "metabolic engineer", modulating the systemic availability of taurine to instruct host immunity [27-29].

A central discovery of this work is the identification of taurine as the interspecies messenger that bridges microbial activity with host nuclear signaling. We delineate a pathway where taurine availability licenses the activation of Foxo1, a master regulator of cellular stress resilience. The consequent induction of the Sesn3/Sod2/Cat antioxidant triad does not merely quench ROS; it fundamentally alters the intracellular redox state required for macrophage repolarization. This positions the Foxo1-ROS axis as a critical "molecular rheostat" that translates metabolic inputs into immunological outcomes.

Notably, our metabolomics analysis highlighted N-Stearoyl Taurine as a top differential metabolite, while our functional rescue experiments utilized free taurine. We postulate that the specific enrichment of *B. pseudolongum* expands the overall bioavailability of

taurine, which may exist in various conjugated forms (such as N-stearoyl taurine) in the gut lumen but is transported into host cells primarily as free taurine via the upregulated TauT transporter. This suggests that N-Stearoyl Taurine may serve as a stable reservoir or biomarker for the flux of taurine metabolism driven by *B. pseudolongum*.

The convergence of this axis on macrophage polarization highlights the remarkable malleability of the innate immune system in response to metabolic cues [30-32]. Our findings demonstrate that the resolution of colitis is strictly contingent upon the shift from a pro-inflammatory M1 to a reparative M2 phenotype. By proving that disruption of the Foxo1 signaling cascade abrogates TMP efficacy, we define the macrophage not merely as an effector of inflammation, but as the primary executive cell that integrates microbial metabolic signals to orchestrate tissue repair.

However, we acknowledge that the definitive establishment of the molecular hierarchy within this axis warrants further genetic dissection. Specifically, while our data implicate taurine influx as the trigger, future studies utilizing Taut-deficient models are necessary to unequivocally verify the obligate requirement of transporter-mediated uptake in the *B. pseudolongum*-driven metabolic dialogue. Similarly, verifying the cell-autonomous function of the antioxidant switch will require myeloid-specific Foxo1 conditional knockout strategies to strictly preclude bystander effects in the reprogramming of macrophage plasticity.

Conclusion

In summary, our findings delineate a pivotal trans-kingdom signaling axis that orchestrates the resolution of ulcerative colitis through the metabolic recalibration of the host-microbe interface. We establish that the therapeutic efficacy of TMP is not intrinsic to the compound itself but is contingent upon its ability to license *B. pseudolongum* as a metabolic engineer, thereby driving taurine-dependent activation of the Foxo1-mediated antioxidant program. This study moves beyond the cataloging of dysbiotic signatures to define a causal molecular circuit-linking commensal metabolism directly to the epigenetic reprogramming of macrophage plasticity. Ultimately,

targeting the *B. pseudolongum*-taurine-Foxo1 axis represents a transformative strategy for restoring intestinal homeostasis, offering a sophisticated alternative to broad-spectrum immunosuppression in the management of inflammatory bowel diseases.

Materials and methods

Experimental models and subject details

Animals and ethics statement

Male C57BL/6J mice (6 weeks old) were purchased from GemPharmatech Co., Ltd. (Nanjing, China). Mice were housed under specific pathogen-free (SPF) conditions in a controlled environment (22 ± 2°C, 50% ± 10% relative humidity, 12-h light/dark cycle) with ad libitum access to standard chow and autoclaved water. Following a 7-day acclimatization period, mice were randomized into experimental cohorts. All animal protocols complied with the Guide for the Care and Use of Laboratory Animals (NIH) and were approved by the Animal Ethics Committee of the Animal Ethics Committee of Nanchang University (**Approval *No.*NCULAE-20240302099**).

Human study participants and sample collection

Fecal samples and matched clinical metadata were obtained from a cohort of 27 hospitalized patients with confirmed UC at The Second Affiliated Hospital of Nanjing Medical University (Nanjing, China). To minimize confounding variables, strictly defined exclusion criteria were applied: patients were excluded if they presented with concomitant gastrointestinal or systemic autoimmune disorders, infectious colitis, or had received antibiotics, corticosteroids, or immunosuppressive therapy within the 30 days preceding enrollment. The study protocol adhered to the principles of the Declaration of Helsinki and was approved by the Institutional Ethics Committee of The Second Affiliated Hospital of Nanjing Medical University (**Approval *No.*FMT-CN-121123**). Written informed consent was obtained from all participants prior to sample collection.

Method details

DSS-induced colitis and pharmacological interventions

To establish the acute UC model, mice were administered 2.5% (w/v) dextran sulfate sodium (DSS; MW 36-50 kDa; MP Biomedicals, MeilunBio; #MB5535) dissolved in

drinking water for 7 consecutive days (Days 0-7), followed by regular water until the study endpoint. Control mice received vehicle drinking water.

For pharmacological studies, mice were randomized into five groups (n = 6–8/group):

1. Control: Vehicle (sterile distilled water) via oral gavage.
2. DSS + Vehicle: DSS induction plus vehicle gavage.
3. DSS + SASP: DSS induction plus Sulfasalazine (SASP; 200 mg/kg/day) suspended in 0.5% CMC-Na.
4. DSS + L-TMP: DSS induction plus low-dose Tetramethylpyrazine (TMP; 20 mg/kg/day) in sterile water.
5. DSS + H-TMP: DSS induction plus high-dose TMP (40 mg/kg/day) in sterile water.

All gavage treatments were administered daily from Day 0 to Day 14. Dosages were selected based on preliminary dose-response assays and previous pharmacokinetic data [33].

Antibiotic depletion and pseudo-germ-free (PGF) model

To assess the microbiota-dependent efficacy of TMP, a pseudo-germ-free model was established using a broad-spectrum antibiotic cocktail (ABX). The ABX solution consisted of Ampicillin (TargetMOI , #CAS69-53-4, 1 g/L), Vancomycin (TargetMOI, #CAS1404-90-6, 0.5 g/L), Neomycin (TargetMOI, #CAS1405-10-3, 0.5 g/L), and Metronidazole (TargetMOI, #CAS443-48-1, 1 g/L) dissolved in sterile physiological saline. Mice received ABX via daily oral gavage (100 μL/mouse) for 7 days prior to DSS induction (Days -7 to 0) and throughout the experimental period to maintain microbial depletion. A 48-hour washout period was observed after the initial 7-day depletion before commencing subsequent microbial interventions [22, 23].

Microbiota reconstitution and fecal microbiota transplantation (FMT)

To dissect specific microbial contributions, ABX-treated mice were subjected to either specific bacterial colonization or FMT. Mice were allocated into six cohorts (n =

10/group), including controls (ABX alone, ABX+DSS) and intervention groups (reconstituted with *Bifidobacterium* or FMT, with/without TMP or Taurine).

***Bifidobacterium* colonization:** Recipient mice were orally gavaged with 200 μL of a live *Bifidobacterium* suspension (5×10^9 CFU/mL; 1×10^9 CFU/mouse) every three days for a total of 24 days (8 administrations). Suspensions were prepared in sterile anaerobic PBS and stored at 4°C for no more than one week [34, 35].

Combination treatments in gnotobiotic settings

For groups receiving combinatorial therapy (e.g., ABX + DSS + TMP + Taurine), TMP (40 mg/kg) was administered daily via oral gavage. Taurine was administered in drinking water at a dose of 5 g/kg.

Colitis induction and pharmacological interventions

Acute colitis was induced by the administration of 2.5% (w/v) DSS dissolved in autoclaved drinking water ad libitum for 7 consecutive days. DSS solutions were freshly prepared daily and shielded from light to prevent degradation. Pharmacological treatments were administered as follows:

- Taurine supplementation: Mice received 0.5% (w/v) taurine dissolved in drinking water for 14 consecutive days（Days 9–23）.
- TMP administration: Tetramethylpyrazine (TMP) was dissolved in sterile distilled water (4 mg/mL) and administered via daily oral gavage at a dosage of 40 mg/kg (100 μL/mouse). Treatment was conducted for 10 days （Days 23–33）.

Control cohorts received vehicle (sterile distilled water) via oral gavage following an identical schedule.

Cell culture

The murine macrophage cell line RAW264.7 was obtained from American Type Culture Collection. Cells were cultured in high-glucose DMEM (CELL RESEARCE, #ZQ100G) supplemented with 15% fetal bovine serum (FBS, CELL RESEARCE,

#ZQ500-S)), 100 U/mL penicillin, and 100 μg/mL streptomycin. Cultures were maintained at 37°C in a humidified incubator with 5% CO_2. All cell lines were routinely tested negative for mycoplasma contamination.

***In vitro* cytotoxicity and viability assays**

Cell viability was assessed using the Cell Counting Kit-8 (CCK-8; Abbkine). RAW264.7 macrophages were seeded in 96-well plates (1×10^4 cells/well) and allowed to adhere for 24 h. Cells were pre-incubated with indicated concentrations of Taurine (1-50 mM) and/or the Foxo1 inhibitor **AS1842856** (MedChemExpress, #HY-100596) (1-40 nM) for 24 h. Subsequently, Lipopolysaccharide (LPS; 1 μg/mL) was added to the culture medium, and cells were co-incubated for an additional 24 h (48 h total treatment duration). Viability was quantified by adding 10 μL CCK-8 reagent per well, incubating for 1-4 h at 37°C, and measuring absorbance at 450 nm using a microplate reader. Viability was expressed as a percentage relative to the vehicle-treated control.

Histopathology and immunohistochemistry (IHC)

Tissue processing and histology:

On Day 16, mice were euthanized, and colonic tissues were harvested, flushed with cold PBS, and fixed in 4% paraformaldehyde (Servicebio) for 24–48 h. Tissues were dehydrated, embedded in paraffin, and sectioned at 5 μm. Sections were stained with Hematoxylin and Eosin (H&E) for structural analysis or Alcian Blue/Periodic Acid-Schiff (AB-PAS) to visualize goblet cells and mucin production.

Histological scoring:

Colitis severity was quantified by two independent pathologists in a blinded manner based on a composite scoring system (Range: 0–15) evaluating four parameters:

1. Inflammation severity (0, none; 1, mild; 2, moderate; 3, severe).

2. Lesion depth (0, none; 1, mucosal; 2, submucosal; 3, muscularis; 4, transmural).

3. Crypt damage (0, intact; 1, basal 1/3; 2, basal 2/3; 3, surface epithelium only; 4, total crypt loss).

4. Lesion extent (1, 1%–25%; 2, 26%–50%; 3, 51%–75%; 4, 76%–100%).

Immunohistochemistry (IHC)

For MUC-2 detection, sections underwent deparaffinization and rehydration, followed by antigen retrieval in Citrate buffer (pH 6.0) at boiling temperature for 15 min. Non-specific binding was blocked with 5% BSA for 1h at room temperature. Sections were incubated with anti-MUC-2 primary antibody (Proteintech, #27675-1-AP, 1:400) overnight at 4°C. Following incubation with HRP-conjugated secondary antibodies, signals were visualized using DAB chromogen. Images were acquired using a Leica DMi8 fluorescence microscope. MUC-2 expression intensity and distribution were quantified using Image-Pro Plus software.

Enzyme-linked immunosorbent assay (ELISA)

Colonic tissue lysates were prepared by homogenizing frozen tissue in RIPA Lysis Buffer (Beyotime, #P0013B). Supernatants were collected after centrifugation at 12,000 × g for 15 min at 4°C. Cytokine levels (TNF-α, IL-1β, IL-10, and TGF-β) were quantified using commercial ELISA kits (Abclonal: #RK00027, #RK00016, #RK00057; Elabscience: #E-EL-M0037) following the manufacturer's protocols. Absorbance was measured at 450 nm using a microplate reader (BioTek), and concentrations were normalized to total protein content determined by the BCA assay.

Immunofluorescence (IF)

Distal colonic tissues were fixed in 4% paraformaldehyde, embedded in O.C.T. compound (Sakura Finetek), and cryosectioned at 8 μm thickness. Sections were washed in PBS, blocked with 0.3% BSA for 1 h at room temperature, and incubated overnight at 4°C with primary antibodies against F4/80 Mouse anti-F4/80 (Proteintech, #29414-1-AP, 1:400). Following washing, sections were incubated with Rhodamine-conjugated goat anti-rat IgG (H+L) secondary antibodies (Proteintech, #SA00001-1;

#SA00001-2, 1:500) for 2 h at room temperature. Nuclei were counterstained with DAPI (Sigma-Aldrich). Images were acquired using an Olympus IX73 fluorescence microscope.

Western blotting

Protein extracts from mouse colonic tissues were prepared using lysis buffer containing protease and phosphatase inhibitors. The lysates were denatured at 95°C for 10 minutes and separated by 8%-15% SDS-PAGE. Subsequently, proteins were transferred to nitrocellulose membranes. After blocking with 5% skim milk, the membranes were incubated overnight at 4°C with the following primary antibodies: Rabbit anti-ZO-1 (Proteintech, #21773-1-AP, 1:2000), Rabbit anti-Occludin (Proteintech, #27260-1-AP, 1:2000), Rabbit anti-Claudin5 (Proteintech, #29767-1-AP, 1:2000), Rabbit anti-Muc-2 (Proteintech, #27675-1-AP, 1:2000), Rabbit anti-CD163 (HUABIO, ER1804-03, 1:2000), Rabbit anti-CD86 (HUABIO, #ET1606-50, 1:2000), Rabbit anti-TGF-β (Proteintech, #26155-1-AP, 1:2000), Rabbit anti-IL-10 (Proteintech, 60269-1-AP, 1:4000), Rabbit anti-IL-6 (Zenbio, #500286, 1:2000), Rabbit anti-TNF-α (HUABIO, #ER65189, 1:2000), Rabbit anti-IL-1β (Proteintech, #16806-1-AP, 1:2000), Rabbit anti-FOXO1 (Affinit, #AF-6416, 1:2000), Rabbit anti-Phospho-FOXO1A (Affinit, #AF-3416, 1:2000), Rabbit anti-TauT (Proteintech, #26725-1-AP, 1:2000), Rabbit anti-SOD2 (Proteintech, #24127-1-AP, 1:5000), Rabbit anti-SESN3 (Proteintech, 84823-3-RR, 1:2000), Rabbit anti-Catalase (Proteintech, #21260-1-AP, 1:2000), Mouse anti-F4/80 (Proteintech, #29414-1-AP, 1:400). Rabbit anti-GAPDH (Proteintech, #10494-1-AP, 1:5000) was used as loading control.

Following primary antibody incubation, membranes were washed with TBST and incubated with HRP-conjugated secondary antibodies (HRP Goat Anti-Rabbit IgG, BIOKER, #H6162, 1:5000; HRP-conjugated Goat Anti-mouse IgG, BOSTER, #BA1050, 1:5000); for 1 hour at room temperature. Protein bands were visualized using enhanced chemiluminescence (ECL, Pierce Chemical Co., Ltd) and imaged.

16S rRNA gene sequencing and microbiome analysis

Microbial DNA was extracted from fecal samples using the E.Z.N.A.® Soil DNA Kit according to the manufacturer's instructions. The V3–V4 hypervariable regions of the 16S rRNA gene were amplified and sequenced on an Illumina HiSeq platform (2 × 250 bp paired-end reads) by Wuhan Metware Biotechnology.

Raw reads were quality-filtered and merged using FLASH (v1.2.11). OTU clustering and taxonomic classification were performed using QIIME (v1.9.1) against the SILVA database (release 138.1). Alpha- and beta-diversity indices were calculated to assess community structure. Differentially abundant taxa were identified using Linear Discriminant Analysis Effect Size (LEfSe) with an LDA score threshold of > 2.0. Functional potential was predicted using PICRUSt2 [36].

Untargeted fecal metabolomics (GC-MS)

Sample preparation:

Lyophilized fecal samples (30 mg) were homogenized in 300 µL of 1 mM NaOH, centrifuged, and the pellet was re-extracted with 200 µL isopropanol. Supernatants were pooled and derivatized using propyl chloroformate/pyridine in a two-step reaction. The derivative was extracted into chloroform, and the organic phase was analyzed.

GC-MS analysis:

Analysis was performed on an Agilent 7890B GC coupled to a 5977A MSD with an HB-5MS capillary column (30 m × 0.25 mm, 0.25 µm). Helium was used as the carrier gas (1.0 mL/min). The temperature gradient was programmed from 50°C to 290°C. Mass spectra were acquired in electron impact (EI) mode (70 eV) over the range m/z 50–600 [37, 38].

Data processing:

Raw data were processed using MS-DIAL for peak alignment and deconvolution. Metabolites were identified by matching mass spectra and retention indices against the NIST and Fiehn libraries. Statistical significance was determined using OPLS-DA (VIP > 1.0) and the Mann-Whitney U test (FDR-adjusted $P < 0.05$).

Transcriptomic analysis (RNA-seq)

Total RNA was extracted from colonic tissues using TRIzol (Solarbio, #15596018CN) and assessed for quality (RIN > 7.0). cDNA libraries were constructed using the NEBNext Ultra RNA Library Prep Kit and sequenced on an Illumina platform (Metware Biotechnology). Raw reads were filtered using fastp and aligned to the Mus musculus reference genome (GRCm39) using HISAT2. Gene expression was quantified as FPKM/TPM using StringTie. Differential expression analysis was performed using DESeq2 ($P < 0.05$, $|\log2FC| > 1$). Kyoto Encyclopedia of Genes and Genomes (KEGG) pathway enrichment was analyzed using Cloud platform tools, with significance defined as FDR < 0.05.

Statistical analysis

Statistical analyses were performed using GraphPad Prism software (version 9.0), and all quantitative data are presented as the mean ± standard error of the mean (SEM). Sample sizes (n) represent biologically independent replicates as specified in the figure legends. Data distribution and variance homogeneity were evaluated using the Shapiro-Wilk and Brown-Forsythe tests, respectively. For comparisons between two groups, statistical significance was determined by an unpaired, two-tailed Student's t-test for parametric data or the Mann-Whitney U test for non-parametric data. For comparisons involving three or more groups, one-way analysis of variance (ANOVA) followed by Dunnett's multiple comparisons test was utilized for parametric data, whereas the Kruskal-Wallis test with Dunn's post hoc test was employed for non-parametric data. A P value of < 0.05 was considered statistically significant, and non-significant differences are explicitly denoted as ns.

Acknowledgments

This study was supported by National Natural Science Foundation of China (*No.* 82560807; 82560565; 82404050), Key Project of the Natural Science Foundation of Jiangxi Province (*No*.20252BAC250152; 20252BAC250125), Youth Project of the Natural Science Foundation of Jiangxi Province (*No*.20252BAC200530), the Scientific and Technological Research Project of the Jiangxi Provincial Department of Education (*No*.GJJ2403619). Jiangxi Provincial Health Commission Science and Technology Program (*No.*SKJP1320242247). Jiangxi Provincial Department of Education Science and Technology Research Project (*No.*GJJ2503436).

Data availability statement

The data that support the findings of this study are available from the corresponding author upon reasonable request. The 16S rRNA data (**PRJNA1397950; PRJNA1397150; PRJNA1397042**) linking to https://www.ncbi.nlm.nih.gov/bioproject/PRJNA1397950 and RNA-sequencing data (**PRJNA1396770**) linking to http://www.ncbi.nlm.nih.gov/bioproject/PRJNA1396770 can be accessed in the Sequence Read Archive (SRA) database of NCBl.

Conflict of interest statement

The authors declare no conflicts of interest.

Ethics statement

The investigation conforms to the principles outlined in the Declaration of Helsinki and was approved by the Ethics Committee of The Second Affiliated Hospital of Nanjing Medical University (**Approval *No.*FMT-CN-121123**). All animal procedures were performed in strict adherence to the protocols approved by the Animal Ethics Committee of Nanchang University (**Approval *No.*NCULAE-20240302099**).

ORCID

Zhijiang Huang: https://orcid.org/0009-0004-9317-0558

Xiaojian Zhu: https://orcid.org/0009-0005-9672-3493

Dan Liu：https://orcid.org/0000-0002-4684-0318

Bo Yi：https://orcid.org/0009-0009-1722-5525

REFERENCES

1. Liang, Yuqing, Yang Li, Chehao Lee, Ziwei Yu, Chongli Chen, and Chao Liang. 2024. "Ulcerative colitis: molecular insights and intervention therapy." *Molecular Biomedicine* 5: 42. https://doi.org/10.1186/s43556-024-00207-w

2. Le Berre, Catherine, Sailish Honap, and Laurent Peyrin-Biroulet. 2023. "Ulcerative colitis." *Lancet* 402: 571-84. https://doi.org/10.1016/S0140-6736(23)00966-2

3. Kobayashi, Taku, Britta Siegmund, Catherine Le Berre, Shu Chen Wei, Marc Ferrante, Bo Shen, and Charles N. Bernstein, et al. 2020. "Ulcerative colitis." *Nature Reviews Disease Primers* 6: 74. https://doi.org/10.1038/s41572-020-0205-x

4. Petracco, Giulia, Isabella Faimann, and Florian Reichmann. 2025. "Inflammatory bowel disease and neuropsychiatric disorders: mechanisms and emerging therapeutics targeting the microbiota-gut-brain axis." *Pharmacology & Therapeutics* 269: 108831. https://doi.org/10.1016/j.pharmthera.2025.108831

5. Luo, Hua, Guiqing Cao, Chun Luo, Dechao Tan, Chi Teng Vong, Yinyue Xu, and Sicen Wang, et al. 2022. "Emerging pharmacotherapy for inflammatory bowel diseases." *Pharmacological Research* 178: 106146. https://doi.org/10.1016/j.phrs.2022.106146

6. Lin, Jianguo, Qingqing Wang, Simin Zhou, Siyu Xu, and Kuiwu Yao. 2022. "Tetramethylpyrazine: a review on its mechanisms and functions." *Biomedicine & Pharmacotherapy* 150: 113005. https://doi.org/10.1016/j.biopha.2022.113005

7. Qi, Mingzhu, Xiaohui Su, Zhuohang Li, Helan Huang, Jingbo Wang, Na Lin, and Xiangying Kong. 2024. "Bibliometric analysis of research progress on tetramethylpyrazine and its effects on ischemia-reperfusion injury." *Pharmacology & Therapeutics* 259: 108656. https://doi.org/10.1016/j.pharmthera.2024.108656

8. Guo, Baojian, Chengyou Zheng, Jie Cao, Fangcheng Luo, Haitao Li, Shengquan Hu, and Simon Mingyuan Lee, et al. 2024. "Tetramethylpyrazine nitrone exerts neuroprotection via activation of PGC-1α/nrf2 pathway in parkinson's disease models." *Journal of Advanced Research* 64: 195-211. https://doi.org/10.1016/j.jare.2023.11.021

9. Hegarty, Lizi M., Gareth-Rhys Jones, and Calum C. Bain. 2023. "Macrophages in intestinal homeostasis and inflammatory bowel disease." *Nature Reviews Gastroenterology & Hepatology* 20: 538-53. https://doi.org/10.1038/s41575-023-00769-0

10. Eming, Sabine A., Peter J. Murray, and Edward J. Pearce. 2021. "Metabolic orchestration of the wound healing response." *Cell Metabolism* 33: 1726-43. https://doi.org/10.1016/j.cmet.2021.07.017

11. Fabre, Thomas, Alexander M. S. Barron, Stephen M. Christensen, Shoh Asano, Kathryn Bound, Matthew P. Lech, and Marc H. Nd Wadsworth, et al. 2023. “Identification of a broadly fibrogenic macrophage subset induced by type 3 inflammation.” *Science Immunology* 8: eadd8945. https://doi.org/10.1126/sciimmunol.add8945

12. Chen, Shanze, Abdullah F. U. H. Saeed, Quan Liu, Qiong Jiang, Haizhao Xu, Gary Guishan Xiao, Lang Rao, and Yanhong Duo. 2023. “Macrophages in immunoregulation and therapeutics.” *Signal Transduction and Targeted Therapy* 8: 207. https://doi.org/10.1038/s41392-023-01452-1

13. Witherel, Claire E., Kimheak Sao, Becky K. Brisson, Biao Han, Susan W. Volk, Ryan J. Petrie, Lin Han, and Kara L. Spiller. 2021. “Regulation of extracellular matrix assembly and structure by hybrid m1/m2 macrophages.” *Biomaterials* 269: 120667. https://doi.org/10.1016/j.biomaterials.2021.120667

14. Weinberg, Samuel E., and Navdeep S. Chandel. 2025. “Mitochondria reactive oxygen species signaling-dependent immune responses in macrophages and t cells.” *Immunity* 58: 1904-21. https://doi.org/10.1016/j.immuni.2025.07.012

15. Cifuentes, Mariana, Hugo E. Verdejo, Pablo F. Castro, Alejandro H. Corvalan, Catterina Ferreccio, Andrew F. G. Quest, Marcelo J. Kogan, and Sergio Lavandero. 2025. “Low-grade chronic inflammation: a shared mechanism for chronic diseases.” *Physiology* 40: 0. https://doi.org/10.1152/physiol.00021.2024

16. Lu, Huilun, Jie Huang, Ya-Chao Wang, Eudald Casals, Gregori Casals, and Muling Zeng. 2025. “Beyond m1/m2: the role of reactive oxygen species in liver fibrosis and immune modulation.” *Redox Biology* 88: 103933. https://doi.org/10.1016/j.redox.2025.103933

17. Tran, Melissa, Jun R. Huh, and A. Sloan Devlin. 2025. “The role of gut microbial metabolites in the t cell lifecycle.” *Nature Immunology* 26: 1246-57. https://doi.org/10.1038/s41590-025-02227-2

18. Lim, Seon Ah, Wei Su, Nicole M. Chapman, and Hongbo Chi. 2022. “Lipid metabolism in t cell signaling and function.” *Nature Chemical Biology* 18: 470-81. https://doi.org/10.1038/s41589-022-01017-3

19. Tao, Shiyu, Jinping Fan, Jingjing Li, Zhifeng Wu, Yong Yao, Zhenyu Wang, and Yujun Wu, et al. 2025. “Extracellular vesicles derived from lactobacillus johnsonii promote gut barrier homeostasis by enhancing m2 macrophage polarization.” *Journal of Advanced Research* 69: 545-63. https://doi.org/10.1016/j.jare.2024.03.011

20. Ou, Haiya, Hongshu Huang, Yiqi Xu, Haixiong Lin, and Xiaotong Wang. 2025. “Systematic druggable genome-wide mendelian randomization to identify therapeutic targets and dominant flora for ulcerative colitis.” *Pharmacological Research* 213: 107662.

https://doi.org/10.1016/j.phrs.2025.107662

21. Wang, Zhuoya, Tian Liu, Li Liu, Jian Xie, Furui Tang, Yimin Pi, and Yuchun Zhong, et al. 2025. “Lactobacillus vaginalis alleviates DSS induced colitis by regulating the gut microbiota and increasing the production of 3-indoleacrylic acid.” *Pharmacological Research* 213: 107663. https://doi.org/10.1016/j.phrs.2025.107663

22. Zhang, Shi-Long, Yu-Qin Mao, Zheng-Yan Zhang, Zhan-Ming Li, Chao-Yue Kong, Hui-Ling Chen, and Pei-Ran Cai, et al. 2021. “Pectin supplement significantly enhanced the anti-PD-1 efficacy in tumor-bearing mice humanized with gut microbiota from patients with colorectal cancer.” *Theranostics* 11: 4155-70. https://doi.org/10.7150/thno.54476

23. He, Ningning, Mengjie Mu, Xiaofang Li, Qingyuan Hao, Kaiwei Chen, Xinnan Zhao, and Yang Sun, et al. 2025. “Gut commensal antibiotic-resistant parabacteroides goldsteinii ameliorates mouse colitis through valine-isobutyrate metabolism.” *Research* 8: 867. https://doi.org/10.34133/research.0867

24. Panyod, Suraphan, Wei-Kai Wu, Yen-Peng Lee, Tzung-Yi Lin, Po-Cheng Kuo, Chen-Syuan Yen, and Yi-Hsun Chen, et al. 2025. “Refining antibiotic cocktail regimens for pseudo-germ-free mice and their impact on gut microbiome and pancreatic tumor proteomics.” *Journal of Advanced Research* https://doi.org/10.1016/j.jare.2025.08.015

25. Kedia, Saurabh, Shubi Virmani, Sudheer K Vuyyuru, Peeyush Kumar, Bhaskar Kante, Pabitra Sahu, and Kanav Kaushal, et al. 2022. “Faecal microbiota transplantation with anti-inflammatory diet (FMT-AID) followed by anti-inflammatory diet alone is effective in inducing and maintaining remission over 1 year in mild to moderate ulcerative colitis: a randomised controlled trial.” *Gut* 71: 2401-13. https://doi.org/10.1136/gutjnl-2022-327811

26. Orea-Soufi, Alba, Jihye Paik, José Bragança, Timothy A. Donlon, Bradley J. Willcox, and Wolfgang Link. 2022. “FOXO transcription factors as therapeutic targets in human diseases.” *Trends in Pharmacological Sciences* 43: 1070-84. https://doi.org/10.1016/j.tips.2022.09.010

27. Cani, Patrice D., Clara Depommier, Muriel Derrien, Amandine Everard, and Willem M. de Vos. 2022. “Akkermansia muciniphila: paradigm for next-generation beneficial microorganisms.” *Nature Reviews Gastroenterology & Hepatology* 19: 625-37. https://doi.org/10.1038/s41575-022-00631-9

28. Davey, Lauren E., Per N. Malkus, Max Villa, Lee Dolat, Zachary C. Holmes, Jeff Letourneau, and Eduard Ansaldo, et al. 2023. “A genetic system for akkermansia muciniphila reveals a role for mucin foraging in gut colonization and host sterol biosynthesis gene expression.” *Nature Microbiology* 8: 1450-67. https://doi.org/10.1038/s41564-023-01407-w

29. Panzetta, Maria E., and Raphael H. Valdivia. 2024. “Akkermansia in the gastrointestinal tract as

a modifier of human health." *Gut Microbes* 16: 2406379. https://doi.org/10.1080/19490976.2024.2406379

30. Li, Mengyuan, Yuhan Yang, Liting Xiong, Ping Jiang, Junjie Wang, and Chunxiao Li. 2023. "Metabolism, metabolites, and macrophages in cancer." *Journal of Hematology & Oncology* 16: 80. https://doi.org/10.1186/s13045-023-01478-6

31. Liu, Pu-Ste, Yi-Ting Chen, Xiaoyun Li, Pei-Chun Hsueh, Sheue-Fen Tzeng, Hsi Chen, and Pei-Zhu Shi, et al. 2023. "CD40 signal rewires fatty acid and glutamine metabolism for stimulating macrophage anti-tumorigenic functions." *Nature Immunology* 24: 452-62. https://doi.org/10.1038/s41590-023-01430-3

32. Li, Mengyuan, Yuhan Yang, Liting Xiong, Ping Jiang, Junjie Wang, and Chunxiao Li. 2023. "Metabolism, metabolites, and macrophages in cancer." *Journal of Hematology & Oncology* 16: 80. https://doi.org/10.1186/s13045-023-01478-6

33. Robles-Vera, Iñaki, Aitor Jarit-Cabanillas, Paola Brandi, María Martínez-López, Sarai Martínez-Cano, Manuel Rodrigo-Tapias, and Marcos Femenía-Muiña, et al. 2025. "Microbiota translocation following intestinal barrier disruption promotes mincle-mediated training of myeloid progenitors in the bone marrow." *Immunity* 58: 381-96. https://doi.org/10.1016/j.immuni.2024.12.012

34. Zhang, Ke, Yangbin Xu, Yining Zheng, Ting Zhang, Yujiang Wu, Yiting Yan, and Yu Lei, et al. 2024. "Bifidobacterium pseudolongum-derived bile acid from dietary carvacrol and thymol supplementation attenuates colitis via cGMP-PKG-mTORC1 pathway." *Advanced Science* 11: e2406917. https://doi.org/10.1002/advs.202406917

35. Chen, Yang, Huiting Fang, Haiqin Chen, Xiaoming Liu, Jianxin Zhao, Catherine Stanton, R. Paul Ross, Wei Chen, and Bo Yang. 2025. "Bifidobacterium inhibits the progression of colorectal tumorigenesis in mice through fatty acid isomerization and gut microbiota modulation." *Gut Microbes* 17: 2464945. https://doi.org/10.1080/19490976.2025.2464945

36. Hempel, Christopher A., Natalie Wright, Julia Harvie, Jose S. Hleap, Sarah J. Adamowicz, and Dirk Steinke. 2022. "Metagenomics versus total RNA sequencing: most accurate data-processing tools, microbial identification accuracy and perspectives for ecological assessments." *Nucleic Acids Research* 50: 9279-93. https://doi.org/10.1093/nar/gkac689

37. Schmid, Robin, Steffen Heuckeroth, Ansgar Korf, Aleksandr Smirnov, Owen Myers, Thomas S. Dyrlund, and Roman Bushuiev, et al. 2023. "Integrative analysis of multimodal mass spectrometry data in MZmine 3." *Nature Biotechnology* 41: 447-9. https://doi.org/10.1038/s41587-023-01690-2

38. Pang, Zhiqiang, Yao Lu, Guangyan Zhou, Fiona Hui, Lei Xu, Charles Viau, and Aliya F.

Spigelman, et al. 2024. “MetaboAnalyst 6.0: towards a unified platform for metabolomics data processing, analysis and interpretation.” *Nucleic Acids Research* 52: W398-406. https://doi.org/10.1093/nar/gkae253

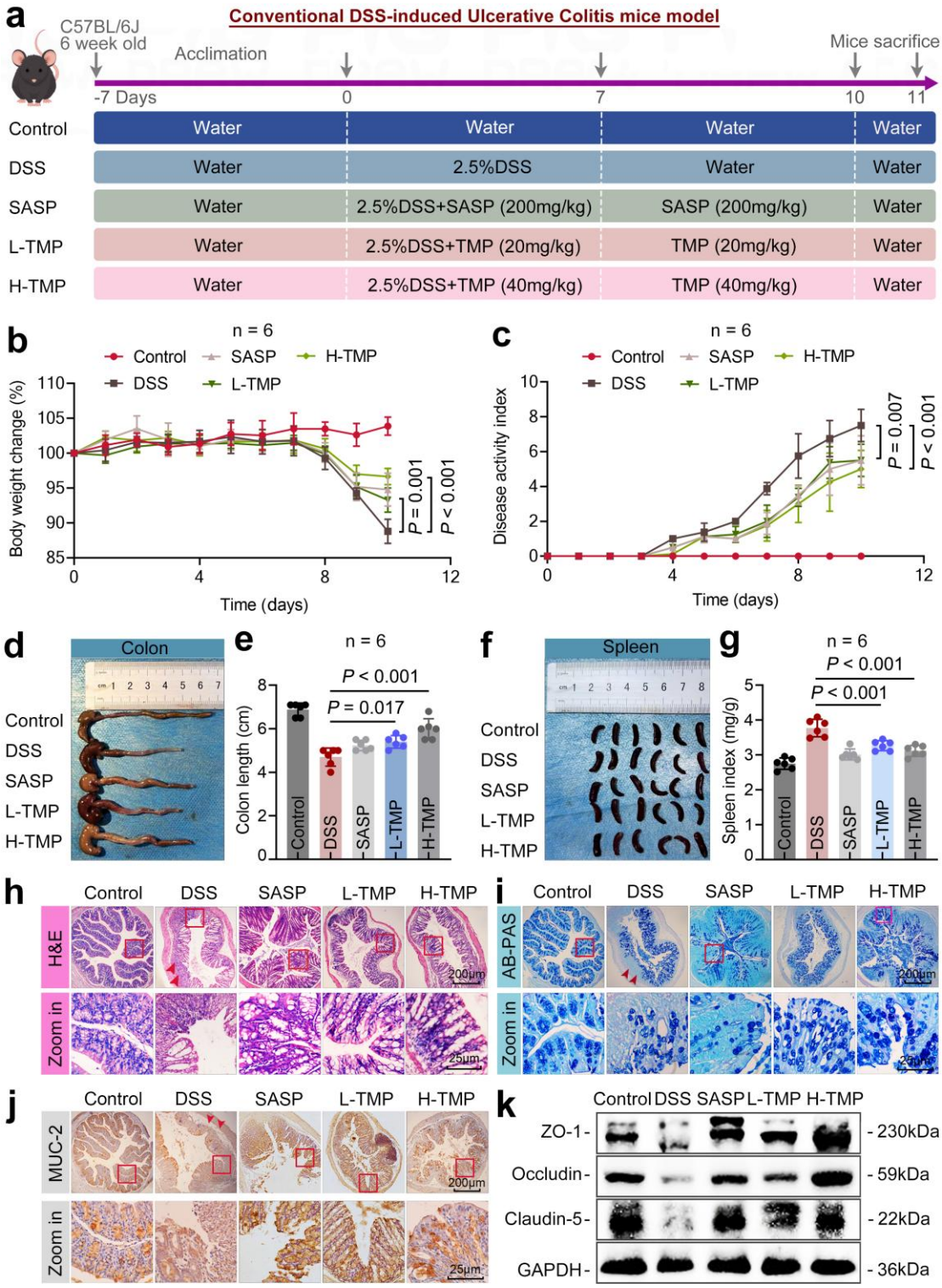


Figure legends

Figure 1. TMP attenuates DSS-induced colitis through intestinal barrier repair.

a. Experimental design. Male C57BL/6J mice (6-week-old, specific pathogen-free) were randomized into six groups (n = 6/group): (1) Vehicle control (0.9% saline), (2)

DSS (2.50% w/v in drinking water, 7 days), (3) DSS + sulfasalazine (SASP, 200 mg/kg/day, i.g., positive control), (4-5) DSS + TMP (20/40 mg/kg/day, i.g.), TMP/SASP treatment was initiated 24 h after DSS induction.

b. Body weight dynamics. Percentage change in body weight relative to baseline (Day 0) was monitored daily. Data represent mean ± SEM (two-way ANOVA with Tukey's post hoc test).

c. Disease progression. Daily disease activity index (DAI) scoring incorporating weight loss, stool consistency, and fecal bleeding (0-4 scale). Data represent mean ± SEM (two-way ANOVA with Tukey's post hoc test).

d-e. Macroscopic pathology. (d) Representative colon specimens showing DSS-induced shortening and (e) quantified colon length (one-way ANOVA with Dunnett's post hoc test).

f-g. Systemic inflammation. (f) Splenomegaly and (g) spleen index (spleen weight/body weight ×1000) as surrogate markers of systemic inflammation (one-way ANOVA with Dunnett's post hoc test).

h-j. Histopathological analysis. (h) H&E-stained colonic sections graded by crypt distortion/inflammatory infiltration (histoscore 0-12). (i) AB-PAS staining for goblet cell density quantification (mucin-producing cells/100 μm crypt). (j) MUC-2 immunohistochemistry (brown: mucin granules; hematoxylin counterstain).

k. Tight junction protein expression. Western blot quantification of ZO-1, Occludin, and Claudin-5 normalized to GAPDH (representative blot from 3 independent experiments). Statistical notation: ns, not significant. Specific tests indicated per panel, Scale bars denote 200 μm and 25 μm unless specified.

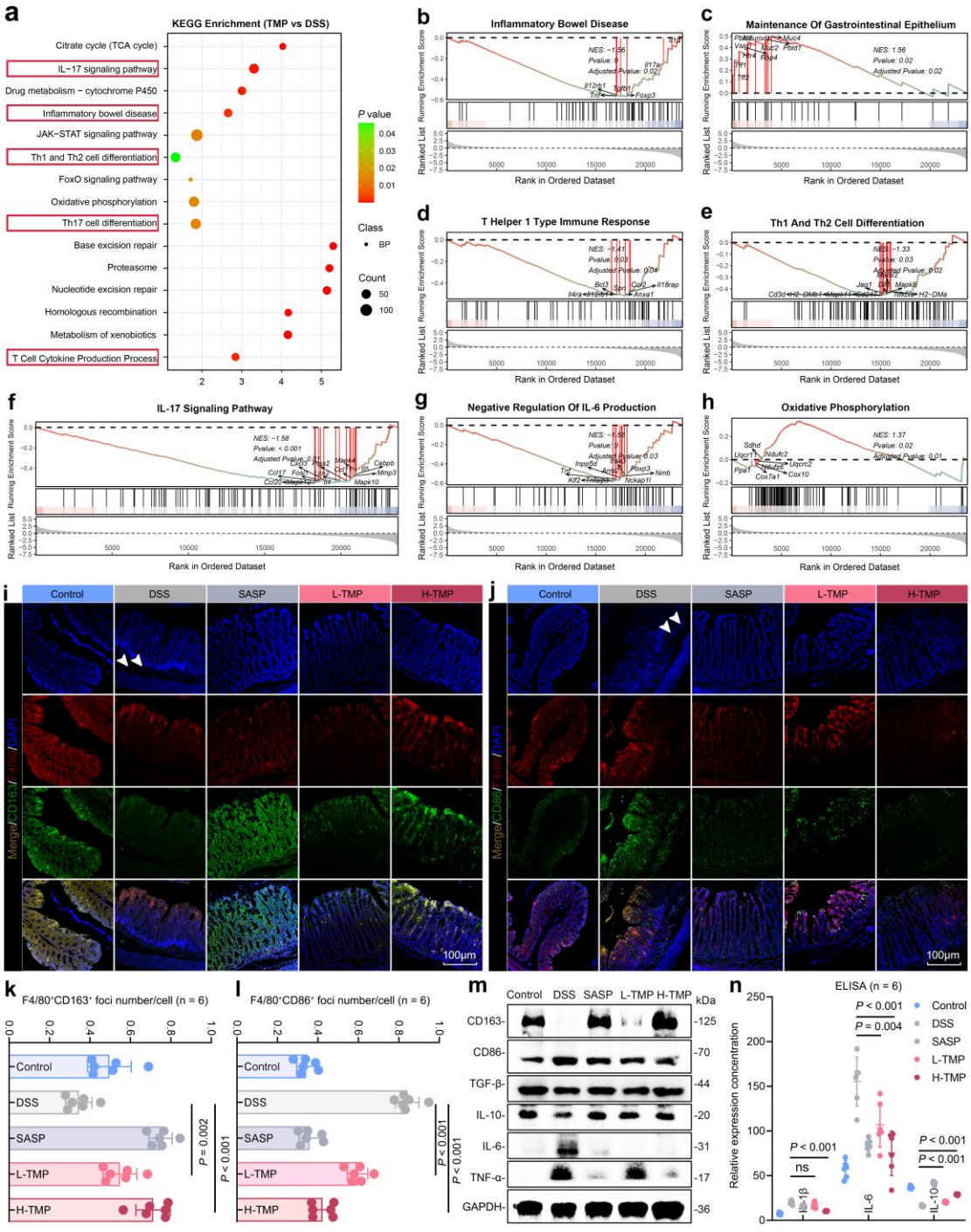


Figure 2. TMP promotes intestinal barrier repair through M2 macrophage polarization in DSS-induced colitis.

a. KEGG pathway enrichment analysis of colonic transcriptomes from TMP- versus DSS-treated mice. Each dot represents a significantly enriched pathway, with dot color indicating the adjusted p value and dot size reflecting the pathway gene count.

b-h. GSEA of the Inflammatory Bowel Disease pathway in TMP- versus DSS-treated

colons. The x-axis represents the rank of genes in the ordered dataset, and the y-axis displays the running enrichment score. The normalized enrichment score (NES), nominal *P* value (NOM *P*), adjusted *P* value (Adj. *P*), and enrichment score (ES) are provided.

i. Immunofluorescence staining of $F4/80^{+}CD163^{+}$ macrophages in colonic sections from the indicated groups (Control, DSS, SASP, L-TMP, H-TMP). CD163 and F4/80 are shown in green and red, and nuclei are stained blue. Scale bar, 100 μm.

j. Immunofluorescence staining of $F4/80^{+}CD86^{+}$ macrophages in colonic sections from the indicated groups (Control, DSS, SASP, L-TMP, H-TMP). CD86 and F4/80 are shown in green and red, and nuclei are stained blue. Scale bar, 100 μm. (one-way ANOVA with Dunnett's post hoc test).

k and l Quantification of $F4/80^{+}CD163^{+}$ and $F4/80^{+}CD86^{+}$ foci per cell in colonic tissues from the indicated groups (one-way ANOVA with Dunnett's post hoc test).

m. Western blot analysis of macrophage markers and cytokines (CD163, CD86, TGF-β, IL-10, IL-6, TNF-α) in colonic tissues from the indicated groups. GAPDH is used as a loading control.

n. ELISA quantification of cytokine concentrations in colonic tissues from the indicated groups (one-way ANOVA with Dunnett's post hoc test).

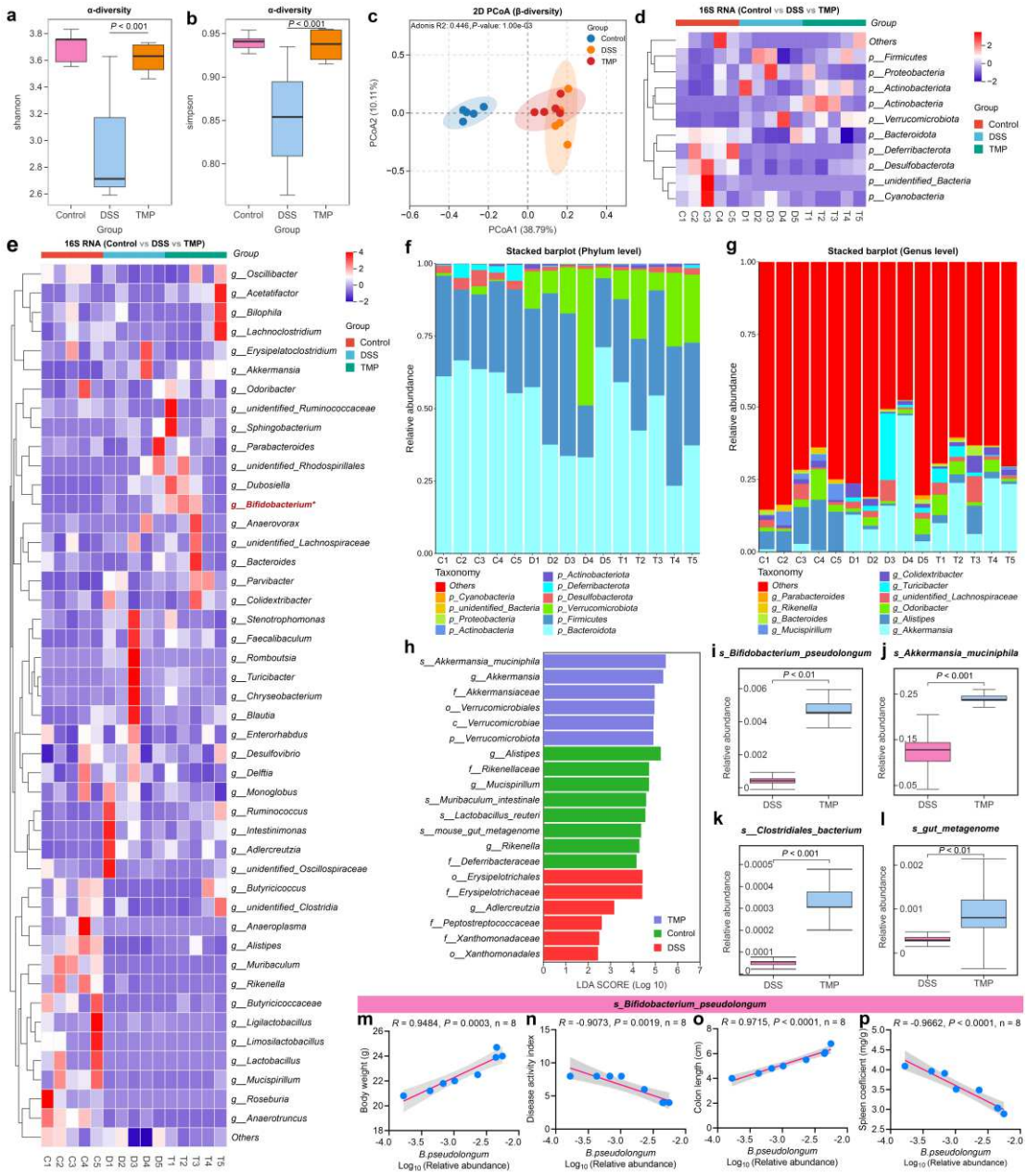


Figure 3. TMP reshapes gut microbial diversity and community structure in DSS-induced colitis.

a. α- diversity of gut microbiota assessed by the Shannon index.

b. α- diversity evaluated by the Simpson index.

c. Principal coordinate analysis (PCoA) of gut microbial communities based on unweighted UniFrac distances.

d. Heatmap of relative abundances at the phylum level across groups.

e. Heatmap of relative abundances at the genus level across groups.

f. Taxonomic composition of gut microbiota at the phylum level in the three groups.

g. Taxonomic composition of gut microbiota at the genus level in the three groups.

h. Histogram of linear discriminant analysis (LDA) effect size (LEfSe) results showing discriminative taxa with LDA score > 4.

i-l. Relative abundances of representative taxa significantly altered between DSS and TMP groups, including ***s_Bifidobacterium_pseudolongum*****,** ***s_Akkermansia_muciniphila*****,** ***s_Clostridiales bacterium*****,** and ***s_gut_metagenome*****.** Data are presented as mean ± SEM (n = 5).

m-p. Correlation analysis between ***B.pseudolongum*** abundance and body weight, DAI, colon length, and spleen index in the TMP-treated mouse model.

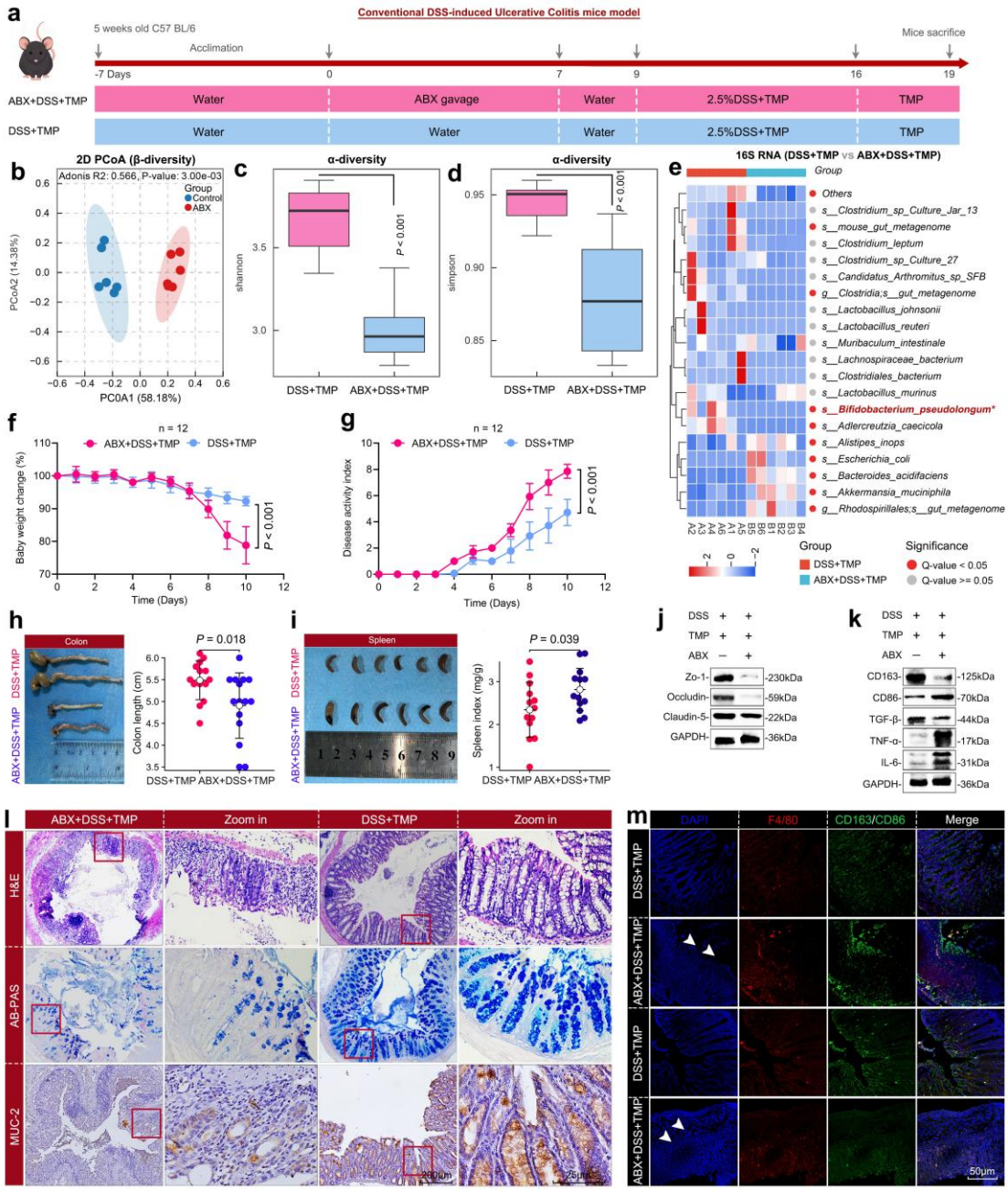


Figure 4. ABX-induced gut microbiota depletion abrogates the therapeutic effect of TMP in DSS-induced colitis mice.

a. Experimental timeline: Schematic representation of the experimental protocol showing the 5-week DSS cycle, ABX administration, and TMP treatment groups.

b. Principal Coordinate Analysis (PCoA): Microbiota composition was assessed via 16S rRNA sequencing. PCoA plots show clustering of microbiota profiles among groups, reflecting significant differences in microbiota diversity and composition.

Adonis $R^2 = 0.566$, P-value < 0.001.

c. α-diversity (Shannon index): Box plots comparing the microbiota diversity (Shannon index) between the DSS+TMP, ABX+DSS+TMP, and DSS groups. The diversity is significantly reduced in the ABX+DSS+TMP group, indicating a loss of microbial richness following ABX treatment.

d. β-diversity (Bray-Curtis dissimilarity): Box plots showing dissimilarity in microbiota composition between the groups. ABX treatment leads to significant shifts in microbiota structure as compared to TMP treatment alone.

e. 16S rRNA sequencing heatmap: Heatmap displaying the relative abundance of key bacterial taxa across the experimental groups. Significant shifts in microbial composition are observed in the ABX+DSS+TMP group. Red denotes higher relative abundance, while blue denotes lower relative abundance.

f. Body weight change: Line graphs tracking the body weight of mice over time. ABX+DSS+TMP-treated mice show significantly greater weight loss compared to DSS+TMP-treated mice, indicating an exacerbation of colitis upon microbiota depletion.

g. Disease activity index: Line graphs depicting disease activity scores over time. ABX-induced microbiota depletion results in a significant increase in disease activity, suggesting that the therapeutic effect of TMP is abrogated in the absence of a healthy gut microbiota.

h. Colon length measurement: Bar graphs comparing the colon length across experimental groups. Colon length is significantly shortened in ABX+DSS+TMP-treated mice, a marker of severe colitis.

i. Spleen index: Bar graphs showing spleen weight (mg) across the groups. ABX+DSS+TMP treatment leads to significantly increased spleen weight, indicating enhanced systemic inflammation.

j. Western blot analysis: Representative immunoblots for tight junction proteins

(Occludin, Claudin-5) and inflammatory markers (CD163, CD86, TNF-α) in colonic tissues. GAPDH is used as a loading control. ABX+DSS+TMP-treated mice exhibit reduced expression of Occludin and Claudin-5, and increased expression of inflammatory markers, indicating impaired barrier function and heightened inflammation.

k. Western blot analysis of immune markers: Immunoblot showing the expression of CD163, CD86, and TNF-α in colonic tissues from DSS and TMP-treated groups, with GAPDH as a loading control. TMP treatment partially restores M2 macrophage polarization and reduces inflammation.

l. Histological analysis (H&E staining): Representative H&E-stained colon sections showing tissue architecture and inflammation. The colon tissues from ABX+DSS+TMP mice exhibit more severe damage and inflammatory infiltration compared to DSS+TMP-treated mice.

m. Immunofluorescence for immune markers: Immunofluorescence staining of colon sections for F4/80 (macrophage marker), CD163 (M2 macrophage marker), and CD86 (pro-inflammatory marker). Merged images show the colocalization of F4/80, CD163, and CD86 in macrophages, indicating altered macrophage polarization in response to TMP treatment in the presence or absence of ABX. Arrowheads point to colocalized foci. Scale bar, 50 μm.

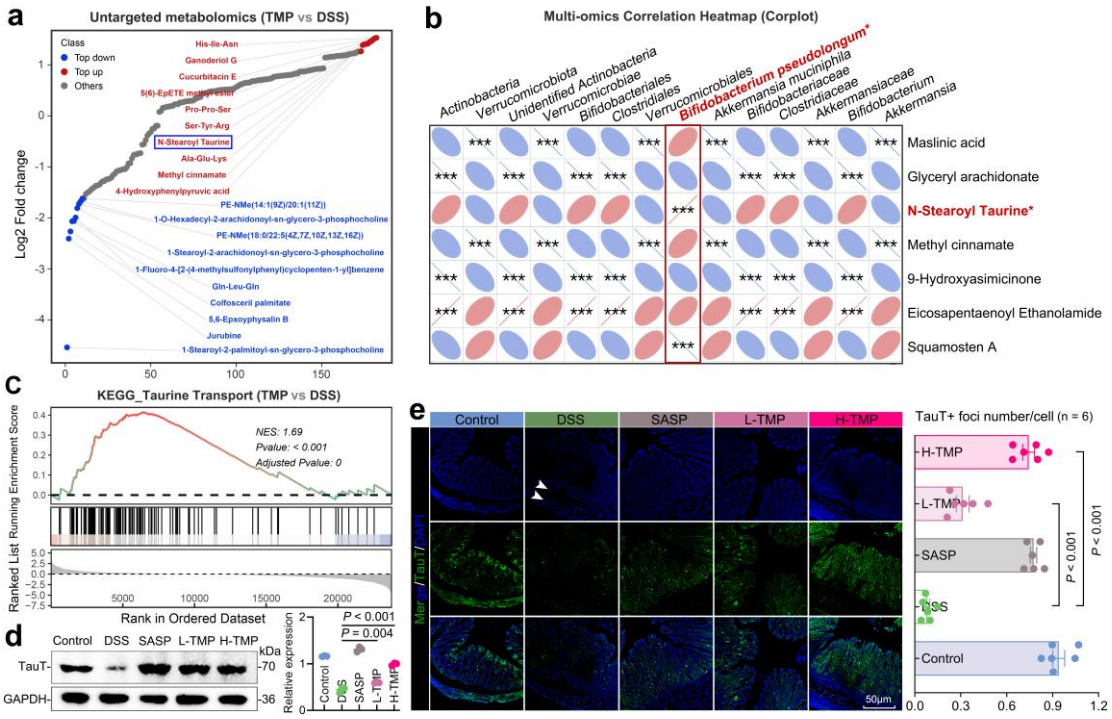


Figure 5. Untargeted metabolomics identifies *B. pseudolongum* as a key regulator of taurine metabolism.

a. Principal component analysis (PCA) score plot showing distinct metabolic profiles between TMP and DSS (n = 5 per group).

b. Multi-omics Correlation Heatmap (Corplot) of Spearman's rank correlation coefficients between microbial genera (phylum-level) and fecal metabolites (n = 5 samples).

c. GSEA plot illustrates the enrichment of genes associated with the KEGG pathway Amino Acid Biosynthetic Process in a ranked dataset. The red line represents the enrichment score (ES) curve, with the peak indicating the highest enrichment of pathway genes. Statistical significance is indicated by NES (Normalized Enrichment Score, 1.34). The bottom panel shows the rank distribution of all genes in the dataset, with the pathway genes (red bars) and non-pathway genes (gray bars) highlighted.

d. Western blot analysis of TauT expression in different groups (Control, DSS, SASP, L-TMP, H-TMP). GAPDH serves as a loading control. The relative expression of TauT is quantified, with statistical significance ($P < 0.05$) indicated.

e. Immunofluorescence (IF) images and quantification of TauT+ foci. IF images (top) show TauT (green) and DAPI (blue) staining in cells from different groups (Control, DSS, SASP, L-TMP, H-TMP). The bar graph (bottom) quantifies the number of TauT+ foci per cell, with statistical significance ($P < 0.05$) indicated. The scale bar (200 μm) is shown in the bottom right corner.

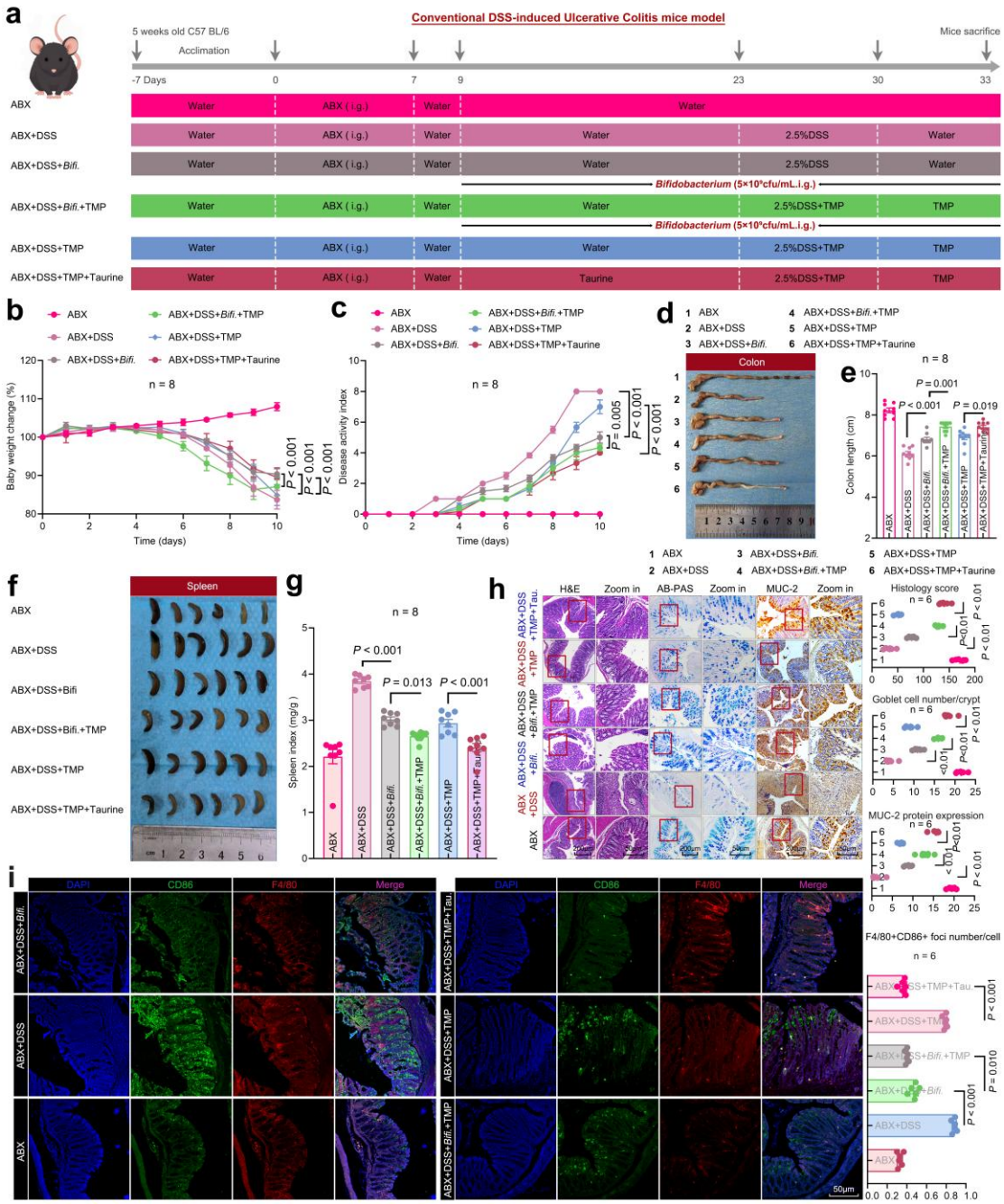


Figure 6. *B. pseudolongum*-derived Taurine alleviates DSS-induced colitis and restores intestinal barrier function by modulating macrophage polarization.

a. Schematic illustration of the experimental design. C57BL/6 mice were pre-treated with an antibiotic cocktail (ABX) followed by DSS induction. Mice were administered *B. pseudolongum* (*Bifi.*), the taurine transport inhibitor TMP, or Taurine as indicated.

b and c. Assessment of colitis severity showing body weight changes (b) and DAI scores (c) over the experimental period.

d and e. Representative macroscopic images of colons (d) and quantification of colon length (e).

f and g. Representative images of spleens (f) and quantification of the spleen index (g) indicating systemic inflammation levels.

h. Histopathological analysis of distal colon sections. Representative images stained with H&E (left), AB-PAS (middle), and immunohistochemistry for MUC-2 (right) are shown. Scale bars, 100 μm (main) and 20 μm (zoom). Right panels show the quantification of histological scores, goblet cell numbers per crypt, and MUC-2 protein expression levels.

i. Representative immunofluorescence images of colonic tissues stained for DAPI (blue), the M1 macrophage marker CD86 (green), and the pan-macrophage marker F4/80 (red). Scale bar, 50 μm. The quantification of **$F4/80^{+}CD86^{+}$** foci per cell is shown on the right.

Data are represented as mean ± SEM. Statistical significance was determined by one-way ANOVA with Tukey's post hoc test (n = 6 mice per group).

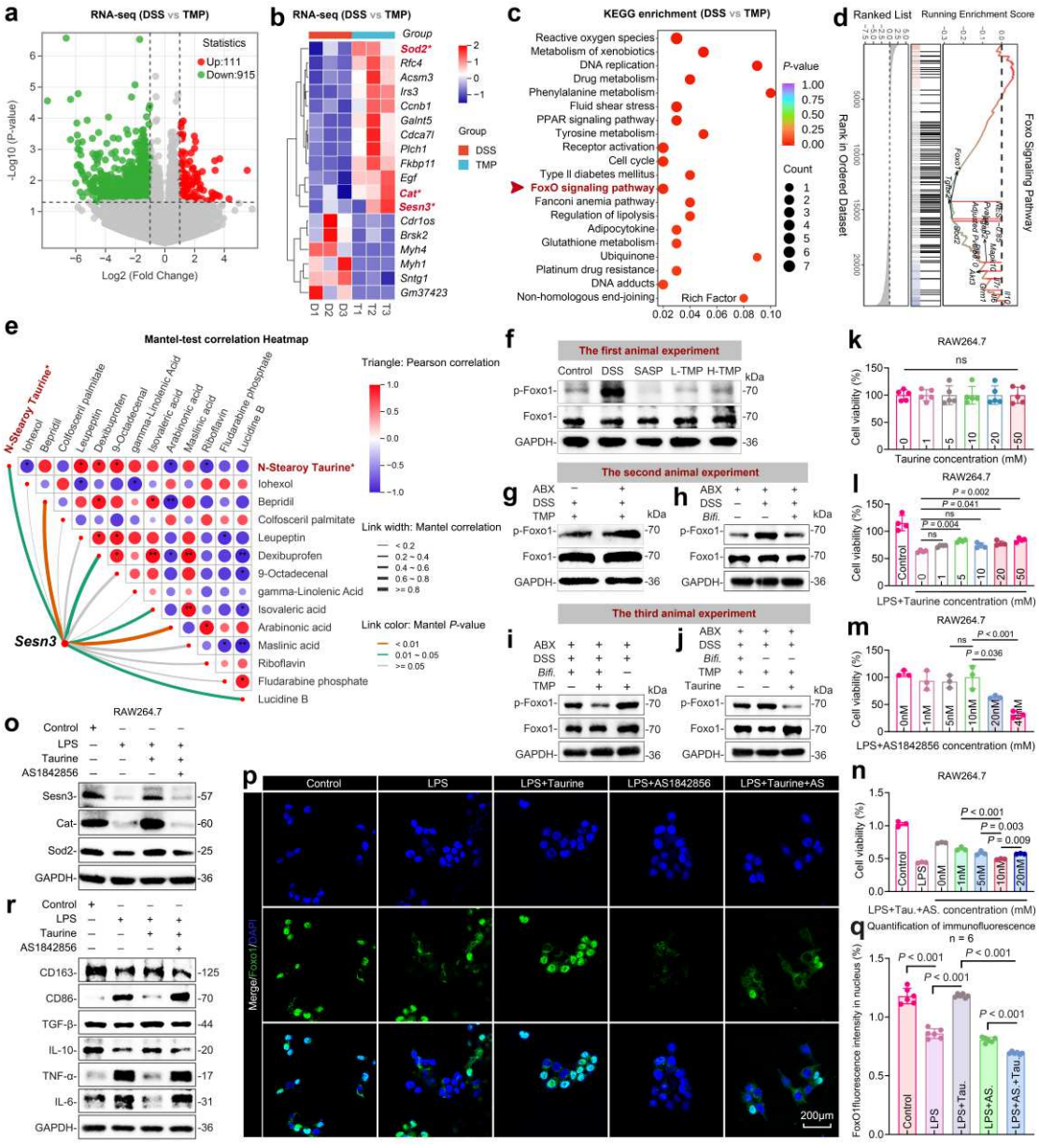


Figure 7. Taurine orchestrates macrophage polarization and resolves inflammation via the Foxo1 signaling axis.

a-d. Transcriptomic profiling of colonic tissues from DSS- and TMP-treated mice. (a) Volcano plot illustrating differentially expressed genes (DEGs). (b) Heatmap visualization of hierarchical clustering for selected DEGs. (c) KEGG pathway enrichment analysis highlighting top dysregulated pathways. (d) GSEA plot demonstrating enrichment of the FoxO signaling signature.

e. Mantel test analysis correlating specific taurine-conjugated metabolites (e.g., N-stearoyl taurine) with key signaling pathway gene sets. Edge width corresponds to

Mantel's r statistic, and edge color denotes statistical significance.

f-j. Immunoblot analysis of p-Foxo1 and total Foxo1 expression in colon tissues. Mice were subjected to different treatment regimens: (f) DSS and TMP treatment; (g and H) antibiotic (ABX) depletion followed by DSS, TMP, or *Bifidobacterium* (*Bifi.*) reconstitution; (i and j) comparison of TMP and Taurine treatment effects in the presence of ABX and *Bifi.*. GAPDH was used as a loading control.

k-n. Cell viability assays in RAW264.7 macrophages treated with varying concentrations of Taurine (k), or challenged with LPS in the presence of Taurine (l), the Foxo1 inhibitor AS1842856 (m), or their combination (n).

o and r. Immunoblot analysis of antioxidant enzymes (Sesn3, Cat, Sod2) (o) and macrophage polarization markers (CD163, CD86, TGF-β, IL-10, TNF-α, IL-6) (r) in RAW264.7 cells under the indicated conditions.

p. Representative immunofluorescence images showing Foxo1 (green) nuclear translocation in RAW264.7 cells. Nuclei were counterstained with DAPI (blue). Scale bar, 200 μm.

q. Quantification of $Foxo1^+$ foci number per cell (n = 6).

Data are represented as mean ± SEM. Statistical significance was determined using one-way ANOVA followed by Tukey’s post hoc test.

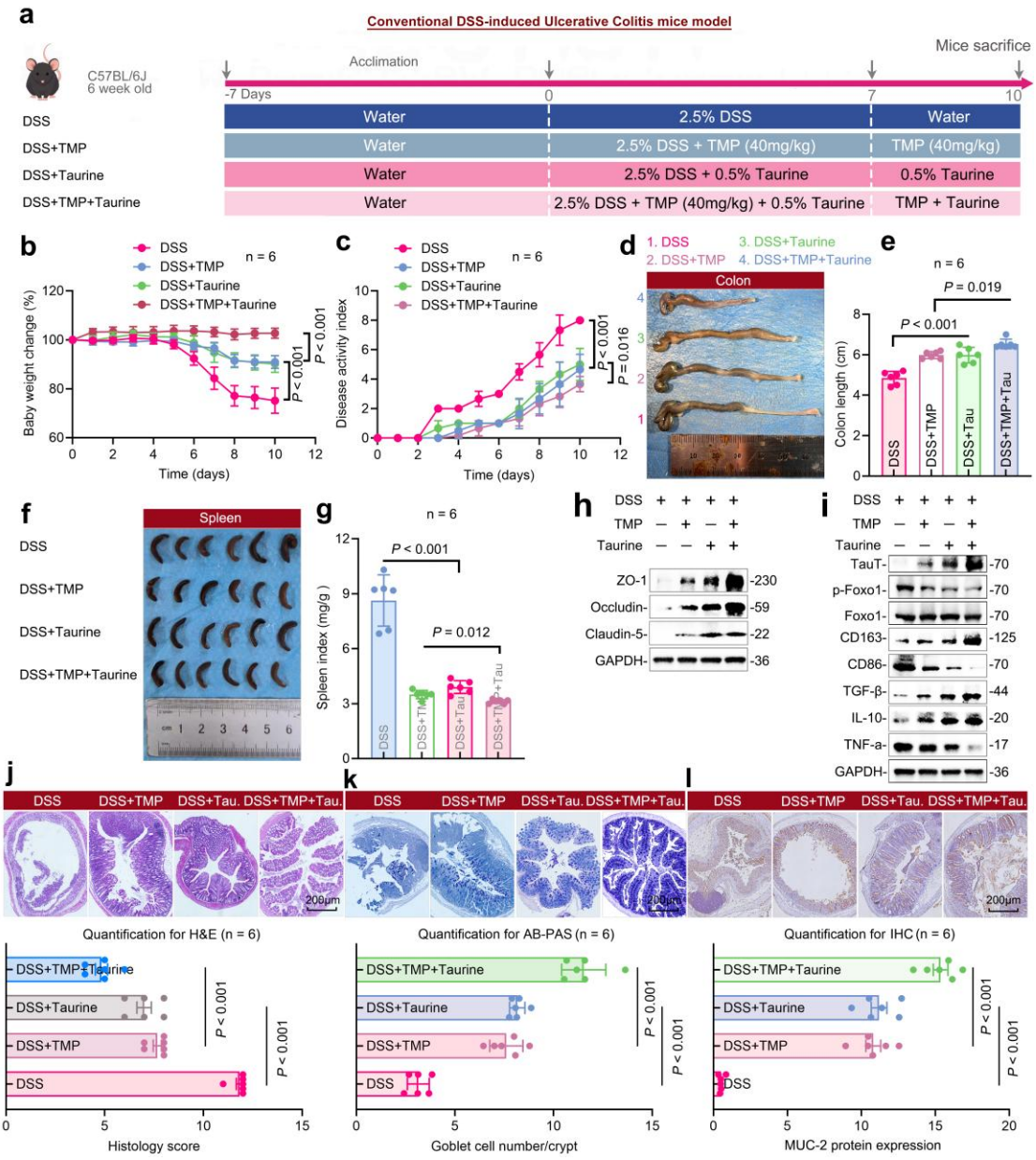


Figure 8. Taurine supplementation recapitulates the protective efficacy of TMP by restoring barrier integrity and modulating macrophage polarization.

a. Schematic illustration of the experimental design. C57BL/6J mice were subjected to DSS colitis and treated with TMP, taurine, or a combination thereof.

b and c. Longitudinal monitoring of body weight changes (b) and DAI scores (c) throughout the experimental course.

d-g. Assessment of macroscopic pathology. Representative images and quantitative analysis of colon length (d and e) and spleen index (f and g).

h and i. Immunoblot analysis of colonic lysates. (h) Expression levels of tight junction proteins (ZO-1, Occludin, and Claudin-5). (i) Assessment of the Foxo1 signaling axis (p-Foxo1, Foxo1), macrophage polarization markers (CD163, CD86), and inflammatory cytokines (TGF-β, IL-10, TNF-α). GAPDH served as the loading control.

j-l. Histological evaluation of colonic tissues. (j) Representative H&E staining with corresponding histological scores based on crypt distortion and inflammatory infiltration. (k) Quantification of goblet cell density via AB-PAS staining. (l) Representative immunohistochemical staining for MUC-2.

Data are represented as mean ± SEM (n = 6 biologically independent animals per group). Statistical significance was determined using two-way ANOVA (for b and c) or one-way ANOVA (for e and g) followed by Tukey's post hoc test.

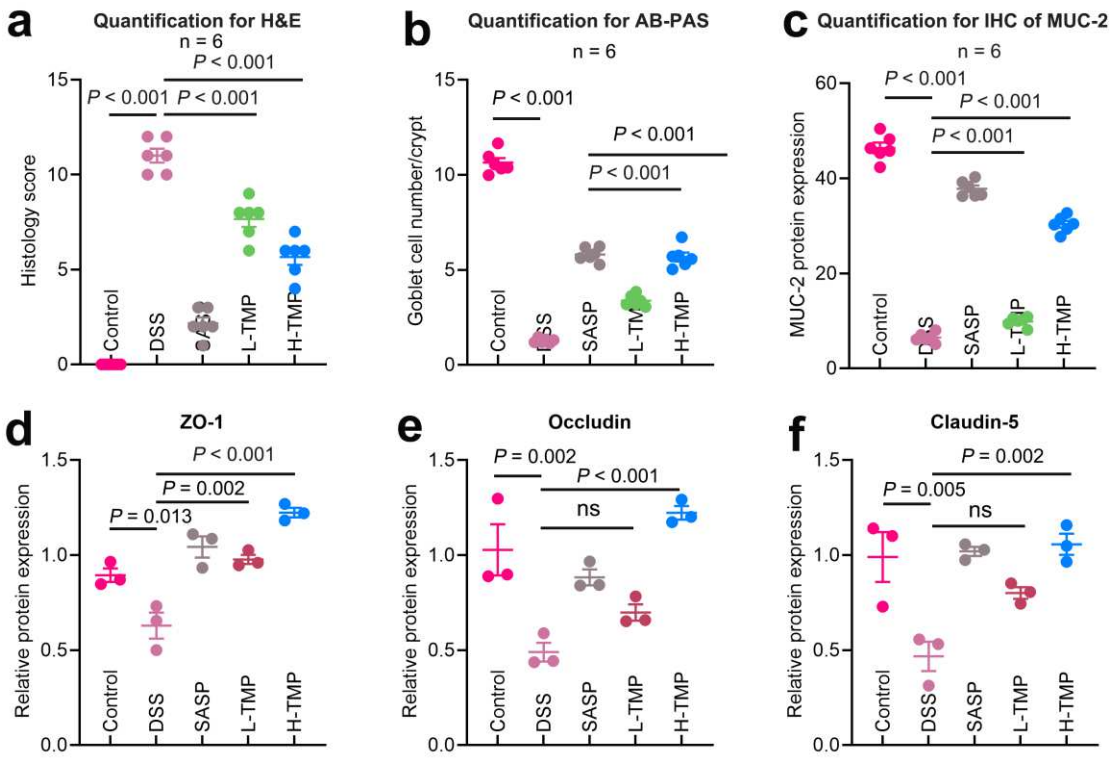


Figure S1. TMP attenuates DSS-induced colitis through intestinal barrier repair, related to Figure 1.

a: Histological assessment of colonic tissue damage quantified by H&E scoring (n = 6).

b: Quantification of goblet cell numbers per crypt assessed by AB-PAS staining, indicating the preservation of mucin-secreting cells (n = 6).

c: Quantitative analysis of MUC-2 protein levels determined by immunohistochemistry (IHC) (n = 6).

d-f: Relative protein expression of the tight junction markers ZO-1 (d), Occludin (e), and Claudin-5 (f) in colonic tissues determined by Western blotting (n = 3).

Data are represented as mean ± SEM. Statistical significance was determined by one-way ANOVA with Tukey's post hoc test.

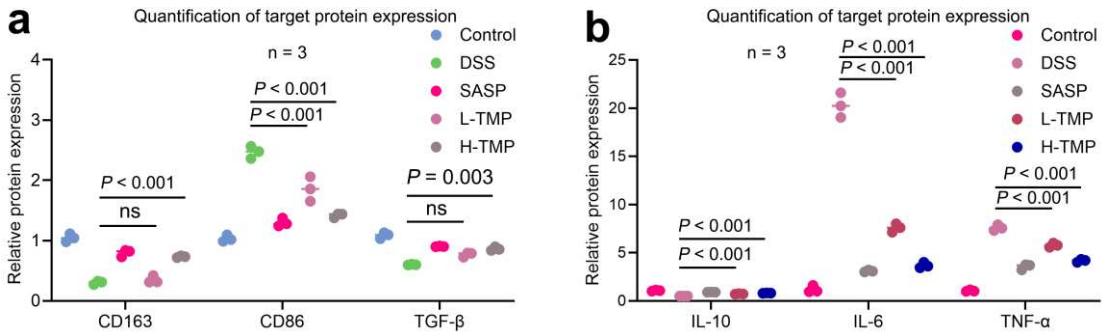


Figure S2. TMP modulates macrophage polarization and cytokine profiles in the colonic tissue, related to Figure 2.

a: Quantification of macrophage functional markers. Relative protein expression of the M2 macrophage marker CD163, M1 macrophage marker CD86, and the anti-inflammatory cytokine TGF-β (n = 3).

b: Quantification of inflammatory cytokine levels. Relative protein expression of the anti-inflammatory cytokine IL-10 and pro-inflammatory cytokines IL-6 and TNF-α (n = 3).

Data are represented as mean ± SEM. Statistical significance was determined by one-way ANOVA with Tukey's post hoc test.

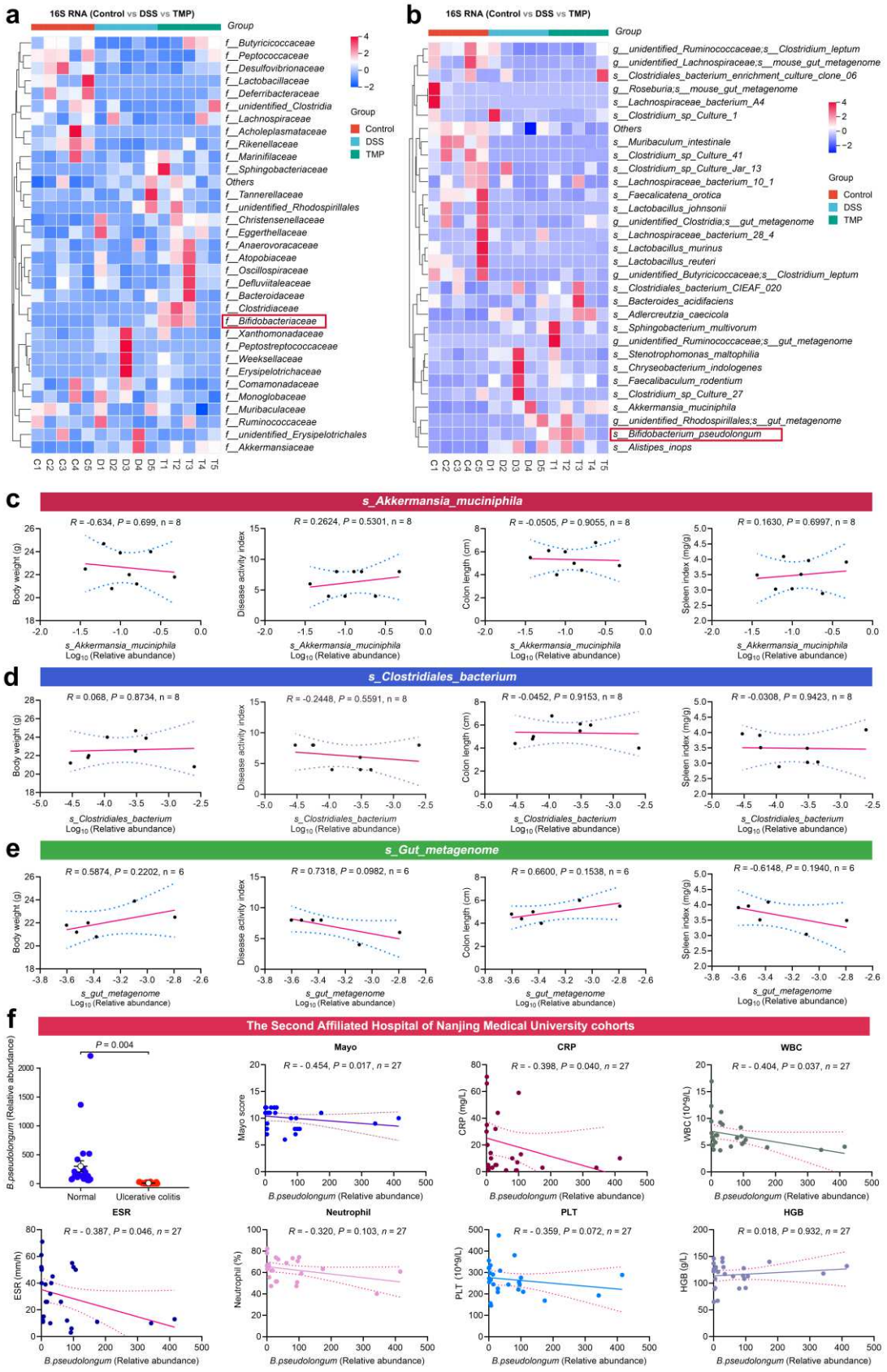


Figure S3. TMP treatment remodels the gut microbiota composition and specific taxa correlate with colitis phenotypes, related to Figure 3.

a and b: Heatmap visualization of the gut microbiota composition at the family (a) and species (b) levels determined by 16S rRNA gene sequencing. The color scale indicates the normalized relative abundance of bacterial taxa across Control, DSS, and DSS+TMP groups. Red boxes highlight the differential abundance of the family Bifidobacteriaceae and species Bifidobacterium pseudolongum..

c-e: Correlation analysis between specific bacterial taxa and host physiological parameters. Scatterplots display the linear regression (solid pink lines) with 95% confidence intervals (blue dotted lines) between the $\log_{10}$-transformed relative abundance of *Akkermansia muciniphila* (c), *Clostridiales bacterium* (d), and *unclassified Gut metagenome* (e) versus body weight, DAI, colon length, and spleen index. Spearman's correlation coefficients and *P* values are indicated (n = 8 biologically independent samples).

f: The relative abundance of *B. pseudolongum* is significantly reduced in UC patients and correlates negatively with inflammatory indices (Mayo score, CRP, WBC, ESR, neutrophils, PLT) while correlating positively with hemoglobin levels (n = 27).

Data are represented as individual points with linear regression lines.

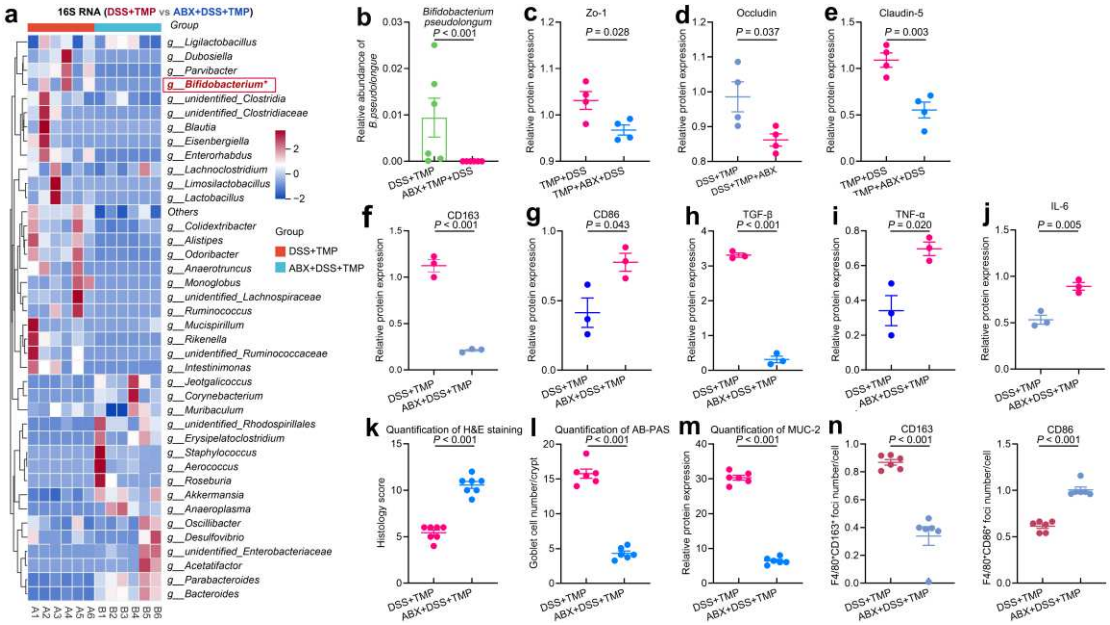


Figure S4. Antibiotic depletion of the gut microbiota compromises the therapeutic efficacy of TMP in DSS-induced colitis, related to Figure 4.

a: Heatmap visualization of the gut microbiota composition at the genus level based on 16S rRNA gene sequencing. The abundance of *B. pseudolongum* (highlighted in red) is notably diminished in the antibiotic-treated group (ABX + DSS + TMP) compared with the DSS + TMP group.

b: Relative abundance of *B. pseudolongum* derived from 16S rRNA sequencing analysis.

c-e: Quantitative analysis of tight junction protein expression in colonic tissues. Relative protein levels of ZO-1 (c), Occludin (d), and Claudin-5 (e) were assessed to evaluate intestinal barrier integrity.

f-j: Quantification of macrophage polarization markers and inflammatory cytokines. Relative protein expression of the M2 macrophage marker CD163 (f), M1 macrophage marker CD86 (g), anti-inflammatory cytokine TGF-β (h), and pro-inflammatory cytokines TNF-α (i) and IL-6 (j).

k: Histological assessment of colonic tissue damage quantified by H&E scoring.

l: Quantification of goblet cell numbers per crypt assessed by AB-PAS staining.

m: uantitative analysis of MUC-2 protein expression determined by IHC.

n: Quantification of macrophage infiltration showing the number of **F4/80^{+}CD163^{+}** and **F4/80^{+}CD86^{+}** foci per cell, assessed by IF.

Data are represented as mean ± SEM. Statistical significance was determined by Student's t-test.

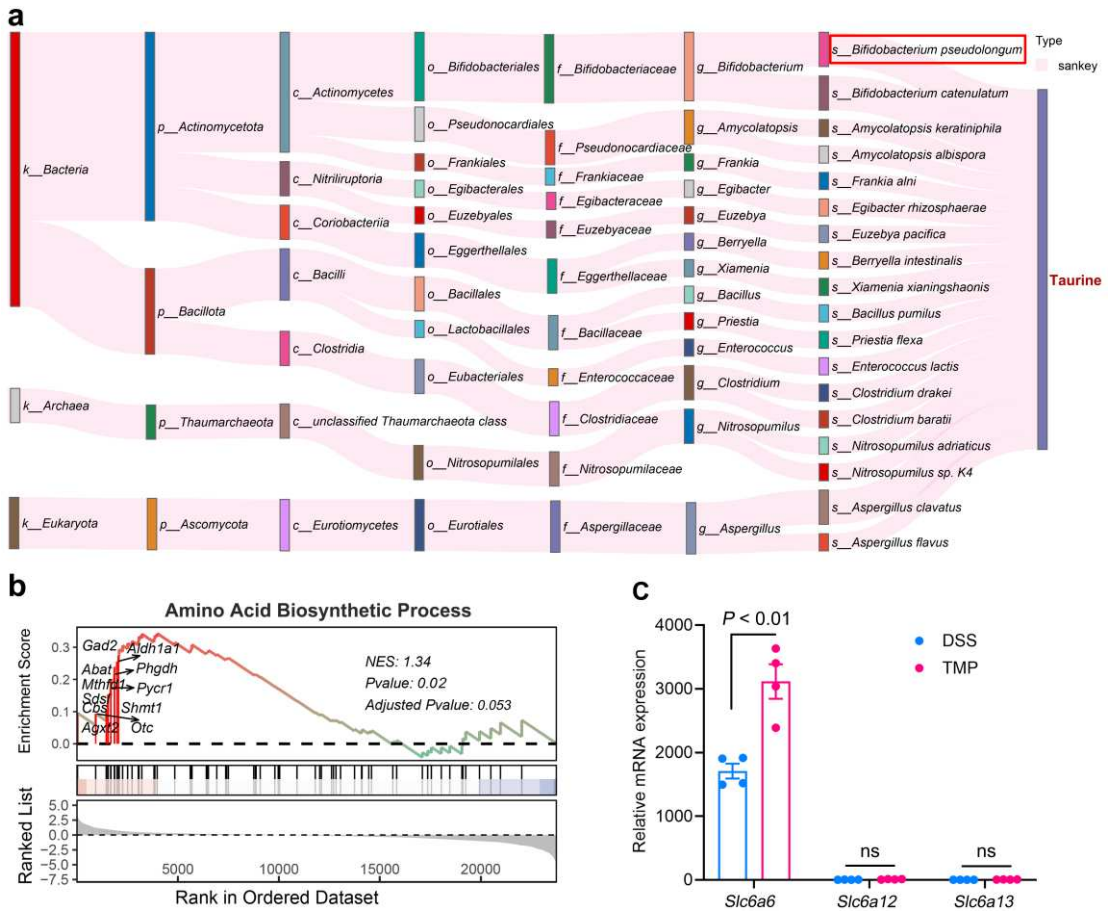


Figure S5. Taxonomic profiling of Taurine-associated microbiota and transcriptional regulation of host amino acid metabolism and taurine transport, related to Figure 5.

a: Taxonomic abundance analysis of gut microbiota (Sankey diagram). Sankey diagram visualization of bacterial taxonomic abundance at the phylum, class, and species levels, reflecting the composition of the gut microbiota in different experimental groups.

b: Enrichment analysis of amino acid biosynthetic processes. Enrichment score plot of the "Amino Acid Biosynthetic Process" pathway, reflecting the enrichment of this pathway in the transcriptome data.

c: Quantitative analysis of mRNA expression. Bar plot showing the relative mRNA expression of *SLC6a6, SLC6a12,* and *SLC6a13* genes, reflecting the expression levels of these genes in different experimental groups.

Data are represented as mean ± SEM (n = 3). Statistical significance was determined

by an unpaired two-tailed Student's t test.

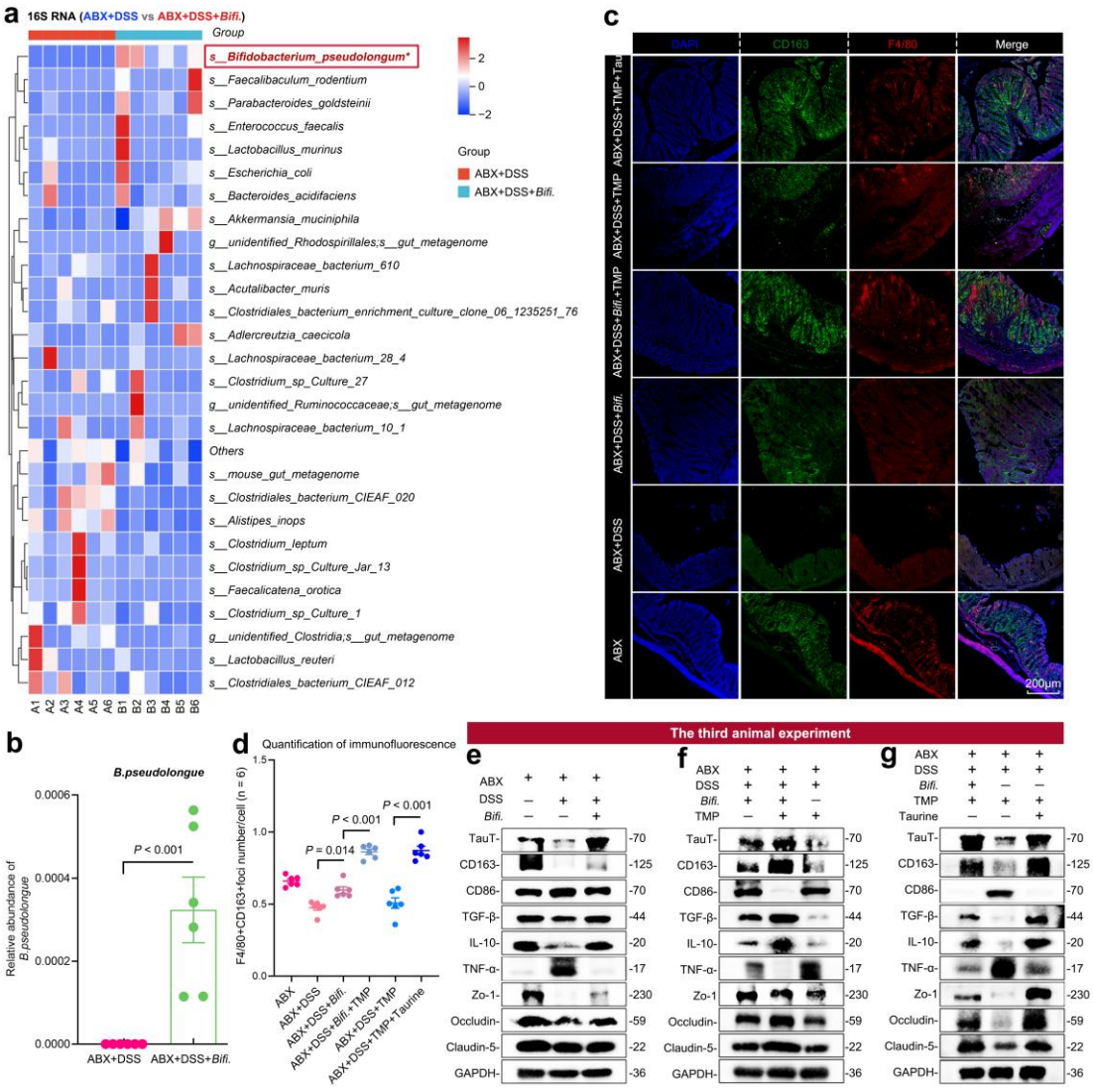


Figure S6. *B. pseudolongum*-derived Taurine alleviates DSS-induced colitis and restores intestinal barrier function by modulating macrophage polarization, relatived to Figure 6.

a: 16S rRNA-seq analysis (ABX+DSS vs ABX+DSS+*Bifi.*). Heatmap visualization of bacterial taxonomic abundance at the species level, reflecting the composition of the gut microbiota in different experimental groups.

b: Quantitative analysis of *B. pseudolongum* abundance. 16S rRNA-seq was used to detect *B. pseudolongum* protein expression, reflecting the abundance of this bacterial species.

c and d: Immunofluorescence staining and quantitative analysis of F4/80^{+}CD163^{+} **macrophage**. Immunofluorescence images show the localization of ZO-1 (green) and Occludin (red) in colonic tissue, with the merged image (yellow) and scale bar (600 μm) provided.

e: Western blot analysis of immune-related proteins. Western blot and quantitative analysis was used to detect the expression of CD163, CD86, TGF-β, IL-10, TNF-α, ZO-1, Occludin, Claudin-5 and GAPDH proteins, reflecting the activation of immune cells and cytokine secretion.

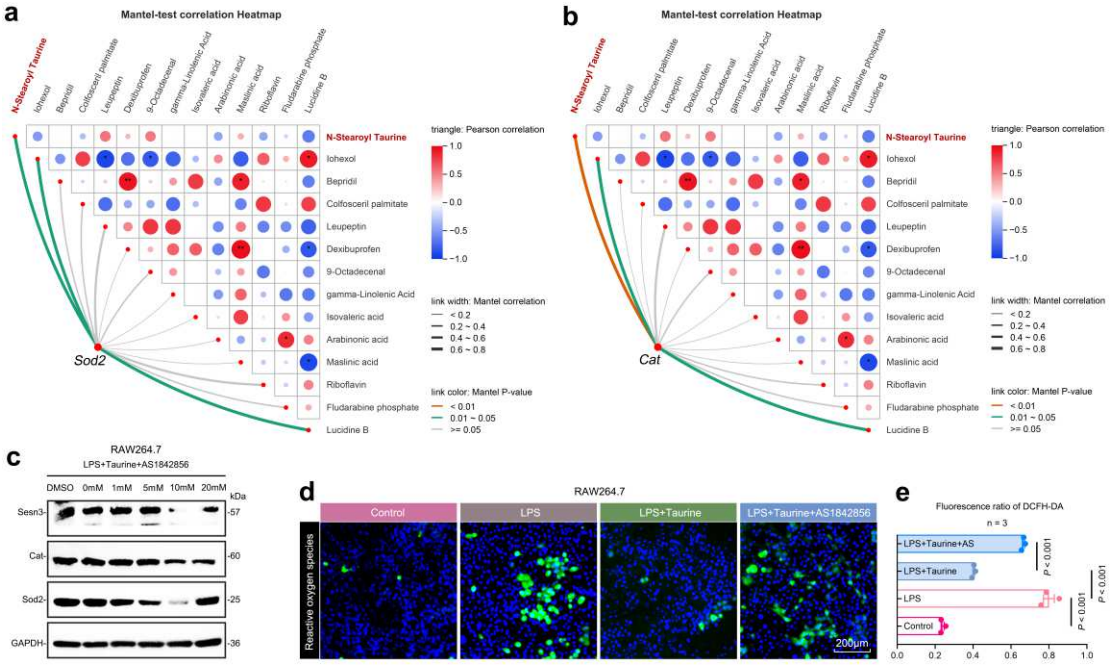


Figure S7. N-stearoyl taurine correlates with antioxidant enzyme expression, and inhibition of foxo1 abolishes taurine-mediated ROS reduction, related to Figure 7.

a and b. Mantel test correlation heatmaps illustrating the regulatory network between specific metabolites and the antioxidant genes (a) *Sod2* and (b) *Cat*. The gradient color of the pairwise heatmaps represents Pearson correlation coefficients between metabolite pairs (n = 3; $P < 0.05$, $P < 0.01$). The curved lines connecting the gene markers (*Sod2* or *Cat*) to specific metabolites denote Mantel test statistics; line width corresponds to the Mantel correlation r-value, and line color indicates the Mantel p-value (orange: $P < 0.01$; green: $0.01 < P < 0.05$; gray: $P < 0.05$). Note the significant correlation of N-Stearoyl Taurine (highlighted in red) with both target genes.

c. Representative Western blots showing the protein expression levels of Sesn3, Cat, and Sod2 in cells treated with LPS and Taurine in the presence of increasing concentrations of the FoxO1 inhibitor AS1842856 (0, 1, 5, 10, and 20 mM). GAPDH was used as a loading control.

d and e. Assessment of intracellular oxidative stress. (d) Representative fluorescence microscopy images of ROS levels detected by DCFH-DA staining (green) across four groups: Control, LPS, LPS + Taurine, and LPS + Taurine + AS1842856 (labeled as AS). Nuclei were counterstained with DAPI (blue). Scale bar, 200 μm. (e) Quantitative analysis of the fluorescence intensity ratio of DCFH-DA from the images in (d).

Data are represented as mean ± SEM (n = 3). Statistical significance was determined by one-way ANOVA with Tukey's post hoc test.